Ratcheting Behavior of a Non-Conventional Stainless Steel and it's Associated Microstructural Variations

Thesis submitted in partial fulfillment of the requirements for the degree

of

Master of Technology
in
Metallurgical and Materials Engineering

Submitted By

Lopamudra Sahu

Roll No- 211MM1368

Department of Metallurgical and Materials Engineering
National Institute of Technology
Rourkela-769008
2013

Ratcheting Behavior of a Non-Conventional Stainless Steel and It's associated Microstructural Variations

Thesis submitted in partial fulfillment of the requirements for the degree of

Master of Technology
in
Metallurgical and Materials Engineering

Submitted By

Lopamudra Sahu

Roll No- 211MM1368

Under Supervision of
Prof. K. Dutta

Department of Metallurgical and Materials Engineering
National Institute of Technology
Rourkela-769008
2013

National Institute of Technology, Rourkela

Certificate

This is to certify that the thesis entitled, **"*Ratcheting Behavior of a Non Conventional Stainless Steel and it's Associated Microstructural Variations*"** submitted by **Miss Lopamudra Sahu** in partial fulfillment of the requirements for the award of the degree of **Master of Technology** in **Metallurgical and Materials Engineering** at the **National Institute of Technology, Rourkela** is an authentic work carried out by her under my supervision and guidance.

To the best of my knowledge, the matter embodied in the thesis has not been submitted to any other University/ Institute for the award of any degree or diploma.

Date:

Place: Rourkela

Supervisor

Prof. K. Dutta

Department of Metallurgical and Materials Engineering

National institute of Technology, Rourkela-769008

Acknowledgements

I would like to express my deep sense of gratitude and respect to my supervisor Prof.K.Dutta, Metallurgical and Materials Engineering Department, NIT Rourkela, for his inspiring guidance, constructive criticism and valuable suggestions throughout the research work. It would have not been possible for me to bring out this thesis without his help and constant encouragement.

I am sincerely thankful to Dr. B.B. Verma, professor Metallurgical and Materials Engineering and other faculty members of this department for their persistent support and advice during the course work.

I am also highly grateful to laboratory members of Department of Metallurgical and Materials Engineering, NIT Rourkela, specially Mr. Hembram, Mr. U.K. Sahu, Mr. A. Pal and Mr. K. Tanty for their help during execution of experiment.

I am thankful to all my classmates and friends who made my stay in Rourkela, an unforgettable and rewarding experience.

Finally, I feel great reverence for all my family members and the Almighty, for their blessings and for being a constant source of encouragement.

Place: Rourkela **Lopamudra Sahu**

Contents

Abstract

The aim of this investigation is to study the influence of asymmetric cyclic loading on accumulation of plastic strain with attendant in-situ microstructural variations that occur during cyclic deformation of a non-conventional stainless steel. The phenomenon of plastic strain accumulation due to asymmetric cyclic loading is known as ratcheting. Stress-controlled cyclic loading experiments have been carried out at 300 K for constant mean stress levels with varying stress amplitudes and constant stress amplitudes with varying mean stress. These tests have been carried out by using a 100 KN servo-hydraulic INSTRON (model: 8500R) testing machine. Cyclic loading rate for stress control test is 50 Mpa/s. The stress, nominal strain and the actuator displacement data were continuously recorded during each test to acquire at least 200 data points per cycle. All fatigue tests have been done upto 50 and 100 number of cycles for further analysis.

To study considerable variation in phases microstructural analyses have been carried out. Transverse sections from the gauge portion of the ratcheted samples have been cut after the cyclic loading tests and were subjected to X-ray diffraction (XRD) analyses using Cu Kα radiation. Microstructural examinations have been done with the help of scanning electron microscope (SEM). In addition, ratcheted samples were investigated to assess any variation of their hardness values. The results highlight that the nature of strain accumulation is dependent on the combinations of means stress and stress amplitude. The results of post-ratcheting hardness tests indicate that there is considerable variation in hardness with number cycles. XRD results indicate that considerable amount of austenite transforms to martensite during ratcheting deformation and the amount of martensite varies with the combination of stresses. Increase in ratcheting strain with increase in mean stress or stress amplitude can be explained from increased plastic damage to the material as well as shifting of zone of plastic deformation.

Key Words: Ratcheting, non-conventional stainless steel, deformation induced martensite, stress amplitude, mean stress.

List of Figures

List of Tables

CHAPTER 1

INTRODUCTION

Introduction

The damage of structural components under various kinds of cyclic loading is a well known engineering problem. Significant efforts are still being laid towards understanding cyclic loading behavior of structural materials by means of studying low cycle fatigue (LCF), high cycle fatigue (HCF) and fatigue crack growth rate (FCGR) behavior. Structural components which are frequently subjected to cyclic loading conditions, where stress approaches to plastic limit of materials, often undergo loading types ranging from symmetric to asymmetric in nature. Ratcheting is the phenomenon of progressive accumulation of permanent deformation when a material is subjected to asymmetric cyclic loading [1,2]; mathematically ratcheting strain can be estimated as average of maximum and minimum strains at a particular cycle during cyclic loading operation [3]. On the other hand it can also be defined as accumulation of plastic strain with the application of cyclic loading characterized by a non-zero mean stress. After sufficient number of cycles, strain becomes such large that original shape of an engineering structure gets altered, thereby making the structure unserviceable. As ratcheting can lead to catastrophic failure of critical components, accurate prediction of this type of deformation is an important issue. During ratcheting, strain may get accumulated till fracture [4] or it may get saturated with increase in number of cycles. According to Jiang et al. [3] ratcheting deformation leads to failure in tension, compression or shear depending on the magnitude of load and initial loading conditions.

Research related to ratcheting deformation of materials has been started around 1911 by Bairstow [5]. However, after Baistow's work, scattered investigations have been done on this field up to about 1960. During 1980's lots of investigations related to ratcheting deformation of materials have been carried out and investigations are still being going on in various systems ranging from metals to alloys, metal matrix composites, solder materials to polymers. These include studies on stainless steel [2, 6, 7], Spring steel [8], carbon steels [3, 9], Sn-Pb solders [10,11], copper and copper alloys [12,13], metal matrix composites [14] and polymers [15,16]. Critical review of all these investigations indicate that these are mainly focused on the development and understanding related to influence of different test

parameters like mean stress [2], maximum stress [2], stress ratio [17], temperature [18] etc, whereas a few of these deal with examining the effect of material behavior like cyclic hardenability and cyclic softenability [19,20]. In the last two decades, some researchers have shown many experimental results on uniaxial and multiaxial ratcheting behavior for SS304 and 316FR [2, 21]. Existing reports suggest that ratcheting behavior depends on types of material, cyclic softening and cyclic hardening behaviors of materials and their loading history [9, 22, 23].

Austenitic stainless steels are class of alloys with a face centered cubic lattice structure of austenite over the whole temperature range from room temperature to the melting point. These steels are used in superheaters and reheaters. For high-temperature boiler applications, three general grades, 304, 321, and 347, are the most widely used. AISI 304LN grade is extensively used in primary heat transport piping systems of advanced heavy water reactors of nuclear power plants. ISO/TR 15510 X12CrMnNiN17-7-5 is a special grade of austenitic stainless steel .This is a non-conventional stainless steel which was developed to conserve nickel and is used in automobile parts such as automotive trim, automobile wheel covers, flat conveyer chains, railroad passenger car bodies. This can be also used in structural members and architectural application such as doors, panels, window and frame. For these applications ratcheting can be considered as an important deformation mechanism. It can be noted that the components of a car must go through different amplitudes of cyclic loading, in their service life, which may be symmetric or asymmetric type. It is therefore a critical issue and emphasis must be given to understand ratcheting and the consequent deformation behavior of X12CrMnNiN17-7-5 stainless steels. During deformation of austenitic stainless steel, austenite transforms to martensite; thus structure of this stainless steel is known to be metastable. There is not much investigations related to microstructural variations during ratcheting and its influence on strain accumulation during ratcheting deformation in the literature. Only a few groups of researchers have studied some substructural variations during ratcheting deformation [24, 25]. Again, microstructural variations during ratcheting have been studied by only a single group [26]. Hence results pertaining to investigations on the ratcheting behavior of X12CrMnNiN17-7-5 stainless steel and corresponding microstructural variations should be of immense importance to improve ratcheting database. In summary,

this investigation incorporates to study the nature of accumulation of plastic strain during ratcheting in X12CrMnNiN17-7-5 stainless steel with suitable characterizations of in situ variations in microstructure and their effect on mechanical properties of the selected material.

1.1 Objectives of the work

The major objectives and relevant work plans to fulfill these can be briefly summarized as:

(i) To characterize microstructures and to determine related mechanical properties of the selected X12CrMnNiN17-7-5 stainless steel:

This part consists of (a) chemical analyses of the selected materials, (b) microstructural characterization of the materials, (c) measurement of grain size and (d) determination of hardness and tensile properties at ambient temperature. Factographic study of the broken tensile specimens has been done to observe there fracture surfaces.

(ii) To study the nature of strain accumulation due to ratcheting in the selected X12CrMnNiN17-7-5 stainless steel:

The major experiments to fulfill this objective are (a) investigations related to asymmetric cyclic loading tests under various combinations of stress amplitude and mean stress in order to examine the nature of accumulation of ratcheting strain at ambient temperature, (b) study of microstructural features for observing the changes occurring in the material due to asymmetric cyclic loading up to 50 and 100 cycles.

(iii) To quantify the volume fraction of transformed phase:

Quantification of volume transform due to ratcheting deformation needs X-ray diffraction analysis. After X-ray diffraction analysis volume fraction of the transformed phases can be estimated by using the relation given in literature survey.

(iv) To examine the variations in post-ratcheting hardness properties:

It is expected that ratcheting deformation would cause improvement/variations in hardness values of the investigated steel. Post-ratcheting hardness tests have been carried out after 50 and 100 cycles of ratcheting deformation.

The thesis has been divided into five chapters. **Chapter-1** deals with the general background of the special grade stainless steel and its applications in the field of structural design. Significance of the problem and the motivation behind this investigation is discussed in this chapter. **Chaper-2** gives a critical review of the existing literature in this field. **Chapter-3** comprises the detail description of the experiments which are being carried out in this investigation. **Chapter-4** includes results and discussion of the present work. **Chapter-5** deals with summary and major conclusions drawn from the present work. Some proposed future works related to this area has been compiled at the end of **Chapter-5**. All the references cited throughout the thesis are enlisted after chapter-5.

CHAPTER 2

LITERATURE REVIEW

Literature Review

2.1 Fatigue-General Concepts

Interest in the prevention of fatigue failure in metallic component began with the advent of industrial revolution where mechanical devices were subjected to repeated loading by the nature of their operation [27]. Fatigue has become progressively more relevant in developed technology in areas, such as automobile, aircraft, compressor, pumps turbine etc. It is well accepted today that all most 90 percent of the all service failure occur due to fatigue. [28].Structural components subjected to repeated cyclic loading and unloading over a long period of time by the nature of their operation, usually fails at stress levels significantly lower than their monotonic fracture strength value. This is commonly known as fatigue failure [29-30]. Three basic factors are necessary to cause fatigue failure. These are

- Maximum tensile stress of sufficiently high values.
- Large enough variation and fluctuation in the applied stress.
- Large number of cycles of the stress applied.

In addition there is a host of other variables, such as stress concentration, corrosion temperature, over loads, metallurgical structure, residual stresses, combined stresses which tend to alter the conditions for fatigue. Fatigue failure is a multi stage process; begins with the initiation of cracks, and with continued cyclic loading the cracks propagate, finally leading to the rupture of a component or specimen. [27].

Ratcheting is a progressive directional accumulation of plastic strain due to asymmetric stress cycling. For a suitable combination of mean stress and stress amplitude, there can be continuous accumulation of plastic strain in every cycle. Studies on ratcheting behavior of materials are limited and research in this domain has gained momentum from last two decades. A brief review of ratcheting behavior of materials is incorporated in different sections of this chapter. Section 2.2 and 2.3 dealt with types of loading and high cycle and

low cycle fatigue respectively. Phenomenological aspect to fatigue life prediction, effect of mean stress on fatigue, cyclic stress-strain response of material and monotonic behavior under tension or compression are discussed in section 2.4, 2.5, 2.6 and 2.7 respectively.

2.2 Types of Loading

Different types of fluctuating load that can cause fatigue are given bellow:

Figure.2.1 (a) illustrates completely reversed cycle of stress of sinusoidal form. For this type of stress cycle the maximum and minimum stresses are equal. In other words we can say symmetric loading ($\sigma_m = 0$). Tensile stress is considered positive and compressive stress is negative. Figure. 2.1(b) represents a repeated stress cycle in which the maximum stress σ_{max} and σ_{min} are not equal.

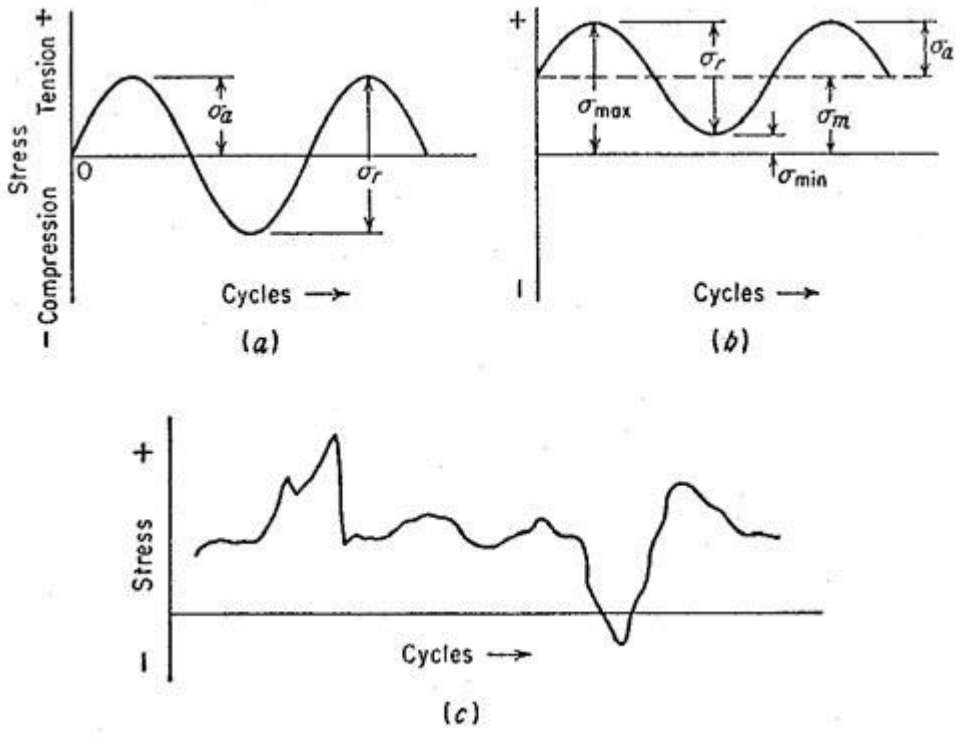

Fig.2.1: (a) Reversed stress cycle (b) Repeated stress cycle (c) Irregular and random stress cycle.

In this figure both σ_{max} and σ_{min} are in tension, but a repeated stress cycle could just as well contain maximum and minimum stresses of opposite signs or both in tension. This is known as asymmetric loading ($\sigma_m \neq 0$). A complicated stress cycle is shown in Figure. 2.1 (c), which

might be encountered in a part such as an aircraft wing which is subjected to periodic unpredictable load due to gusts.

2.3 High cycle fatigue and Low cycle fatigue

Depending on the number of cycles (N) that a material can withstand before failure; fatigue can be categorized into two broad regimes, namely high cycle fatigue (HCF) and low cycle fatigue (LCF). When $N \geq 10^5$ cycles, type of failure can be categorized as HCF and when $N < 10^4$ or 10^5, it is called LCF.

2.3.1 High cycle fatigue (LCF)

In high cycle fatigue, the life is usually characterized as a function of the stress range applied, and the components fail after a high numbers (usually higher than 10^6 cycles) of cycles at a relatively low stress (usually less than 30% of the yield stress) and the deformation experienced is primarily elastic. High cycle fatigue must consider during design of automobiles, aircraft, compressors, pumps and turbines etc where vibration occur. In high-cycle fatigue situations, materials' performance is commonly characterized by S-N curve [Figure.2.2 (a)], a plot indicating the

magnitude of cyclic stress (S) against cycles to failure (N) in logarithmic scale. The S-N curve is sometimes described by Basquin equation

$$N\sigma_a^{\,p} = C \qquad (2.1)$$

Where, σ_a = stress amplitude

p and C are empirical constant.

N= number of cycles to failure

In S-N curve the values of stress that is plotted can be stress amplitude (σ_a) maximum stress (σ_{max}) and minimum stress (σ_{min}).The stress values are usually nominal stresses i,e there is no adjustment for stress concentration. The S-N relationship is determined for a specified value of σ_m stress ratio ($R= \sigma_{min}/\sigma_{max}$) and stress amplitude ($A= \sigma_a/\sigma_m$).

For determinations of the S-N curve, the usual procedure is to test the first specimen at a high stress where failure is expected in a fairly short number of cycles, e.g., at about two-thirds the static tensile strength of the material. The test stress is decreased for each succeeding specimen until one or two specimens do not fail in the specified numbers of cycles, which is usually at least 10^7 cycles. This method is used for presenting fatigue failure in high cycles ($N > 10^5$).

There exists a particular level of stress below which a material can withstand infinite number of cycles without failure. This stress level is known as fatigue limit or endurance limit. Several ferrous systems fall under this category. To the contrary, non-ferrous systems, particularly aluminum and aluminum-based alloys do not possess any well-defined level of stress below which these materials do not fail and therefore, it is critical to define endurance limit for non-ferrous systems. This curve is used to predict the number of cycles sustained under certain stress before failure. The curve gives designers a quick reference of the allowable stress level for an intended service life.

2.3.2 Low cycle fatigue (LCF)

When stress is high enough for plastic deformation to occur, the description of fatigue behavior in terms of stress is less useful and strain in the material offers a smaller description. So in LCF the opposite applies, where life is nominally characterized as a function of the strain range and the component fails after a small number of cycles at a high stress, and the deformation is largely plastic. Strain controlled cyclic loading is found in thermal cycling, where a component expands and contracts in response to fluctuations in the operating temperature. The usual way of presenting low-cycle fatigue test results is to plot the plastic strain range $\Delta\varepsilon p$ against N. This graph is plotted in log-log coordinates is shown in Figure. 2.2 (b). , according to Coffin-Manson relation:

$$\frac{\Delta\varepsilon_p}{2} = \varepsilon_f^{'}(2N)^{C_1} \qquad (2.2)$$

Where:

$\Delta\varepsilon_p /2$ is the plastic strain amplitude;

ε_f' is an empirical constant known as the fatigue ductility coefficient, the failure strain for a single reversal;

2N is the number of reversals to failure (N cycles);

C_1 is an empirical constant known as the fatigue ductility exponent, commonly ranging from -0.5 to -0.7 for metals.

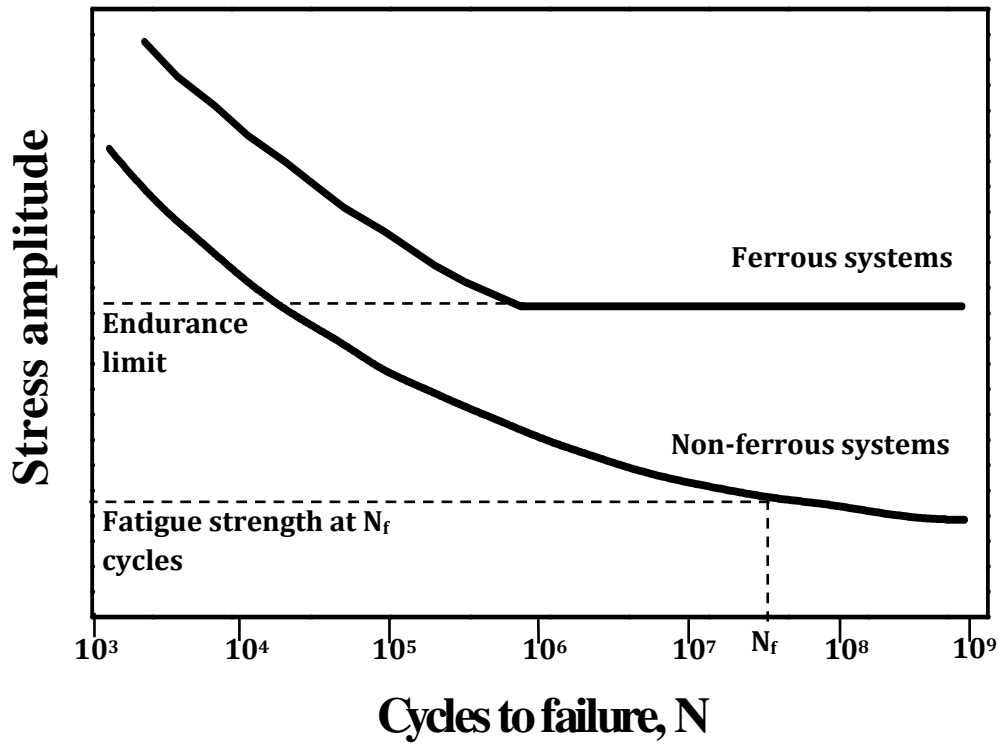

Fig. 2.2 (a): Schematic representation of the S-N curve

Low cycle fatigue is commonly considered during design of nuclear pressure vessels, steam turbines and other type of power machineries, structures where seismic loadings are implemented and so on.

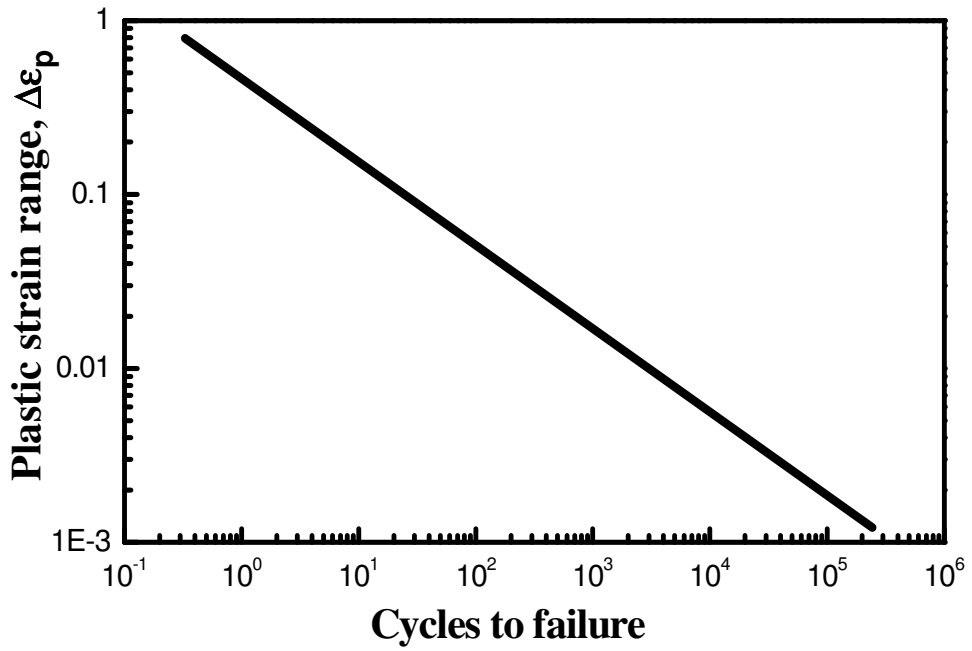

Figure 2.2 (b) : Low cycle fatigue curve ($\Delta\varepsilon_\pi$ vs. N).

2.4 Effect of mean stress on Fatigue

There are large numbers of fatigue data in literature for conditions of zero mean stress (completely reversed stress cycle). There are several methods of determining an S-N diagram for a situation where the mean stress is not equal to zero. The alternating stress is plotted against mean stress in Figure.2.3. This figure shows the formulations that are used to take account of mean stress in describing the fatigue endurance limit. Figure.2.3 is known as the Haig-Soderberg diagram.

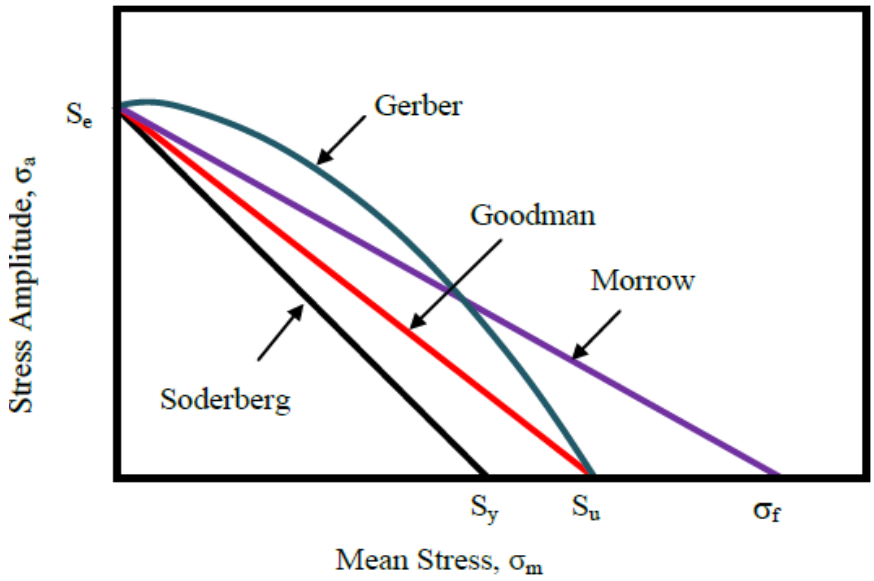

Fig. 2.3: Effect of mean stress on alternating stress amplitude at

The mathematical formulations for the various curves in Figure. 2.3 are:

Morrow: $(\sigma_a/\sigma_e) + (\sigma_m/\sigma_f) = 1$ (2.3)

Gerber: $(\sigma_a/\sigma_e) + (\sigma_m/\sigma_m)^2 = 1$ (2.4)

Goodman: $(\sigma_m/\sigma_e) + (\sigma_m/\sigma_u) = 1$ (2.5)

Soderberg: $(\sigma_a/\sigma_e) + (\sigma_m/\sigma_y) = 1$ (2.6)

Where

σ_a= Stress amplitude.

σ_m =Mean stress

σ_m=Yield stress

σ_u = Ultimate tensile stress

In general, all these relationships show that with increase of mean stress the alternating stress amplitude required for fatigue endurance limit gradually decreases. The Goodman relation gives good result for brittle materials and conservative results for ductile materials. The Gerber relation will give good results for ductile material. Fatigue strength of a component tends to increase with a compressive mean stress and decrease with a tensile mean stress. Gerber's parabolic relationship may therefore yield erroneous answer to the conservative side in the compressive mean stress region.

2.5 Cyclic Stress-strain response of material-Transient behavior

Various factors such as rate of loading, environment, and temperature affect the stress-strain relationship. When a specimen is subject to cyclic loading, the response will differ depending upon the mode of controlled variable as shown in Figure.2.4. [27] The response could be cyclic hardening or cyclic softening, if the experiments are strain-control. There may be mean stress relaxation, if mean stress is present. On the other hand, for fully-reversed stress controlled loading, material may get strain hardening or softening similar to the strain-controlled condition. The plastic strain decreases with the number of cycles and reaches a stable state for strain-hardenable materials and the reverse occur for strain-softenable materials. If the control variable is stress, the response differs and it is a symmetric loading; in this case, the material response is yet to be clearly established. There will be additional strain accumulation due to presence of non-zero mean stress, in each cycle of loading. This phenomenon is commonly known as ratcheting [1, 2, 7, 9, 10, 16, 17, 19, 31- 33] but has also been referred as cyclic creep or cyclic creep strain by a few investigators (12, 24]. In this investigation, it is referred as 'ratcheting' only.

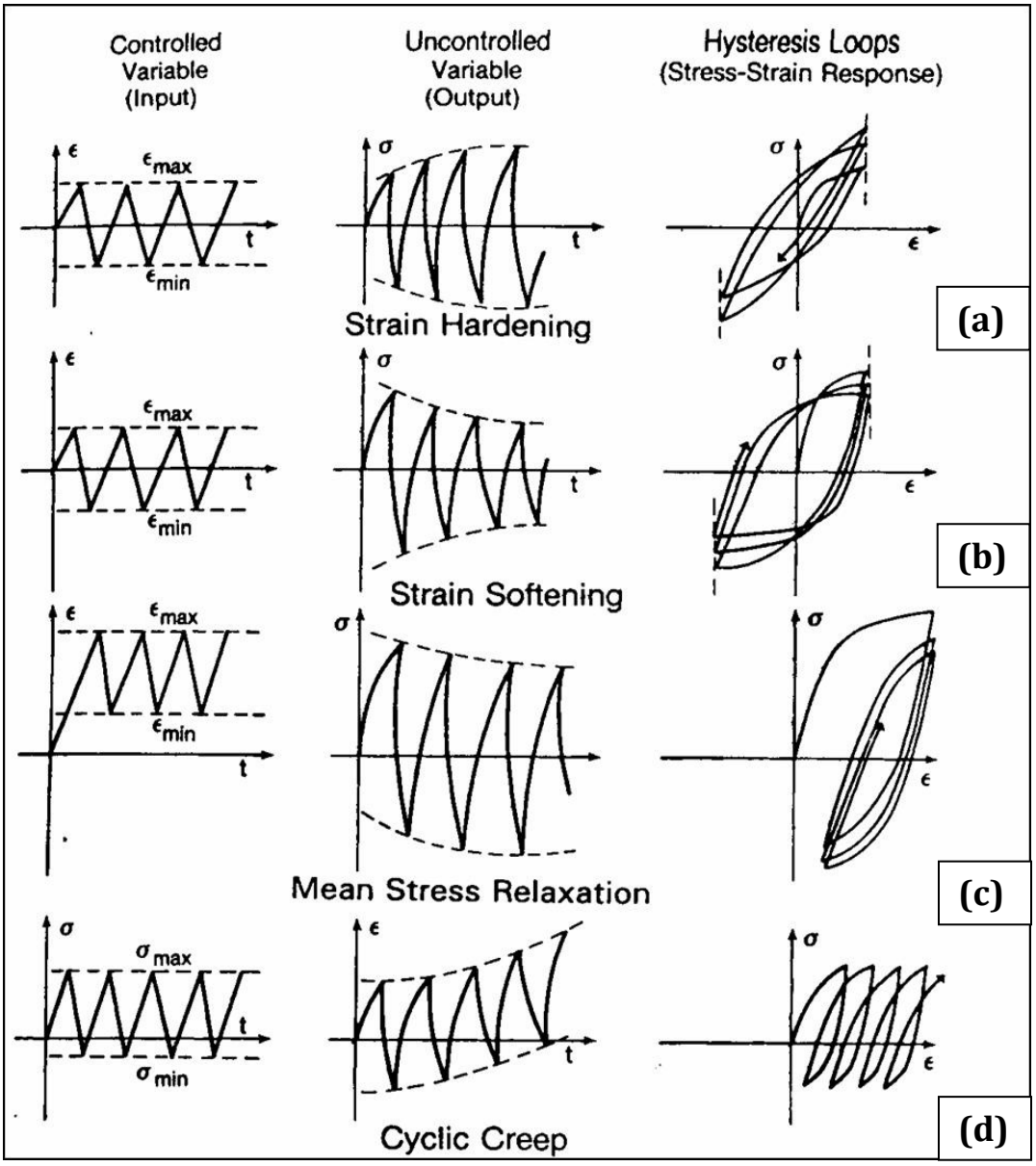

Fig. 2.4: Schematic response to various modes of cyclic input variables (deformation or stress controlled tests) .

2.6 Ratcheting Phenomenon

Ratcheting occurs when asymmetrical cyclic loading is applied to structural components. In each cycle of loading hysteresis loops are known to form. Figure.2.4. shows that the nature of hysteresis loops changes with increase in number of cycles. Ratcheting deformation occurs in such a way that the hysteresis loops produced for subsequent cycles translate towards higher plastic strain direction. The phenomenon is symmetrically illustrated in Figure. 2.4(d) and clarified briefly in Figure.2.5.

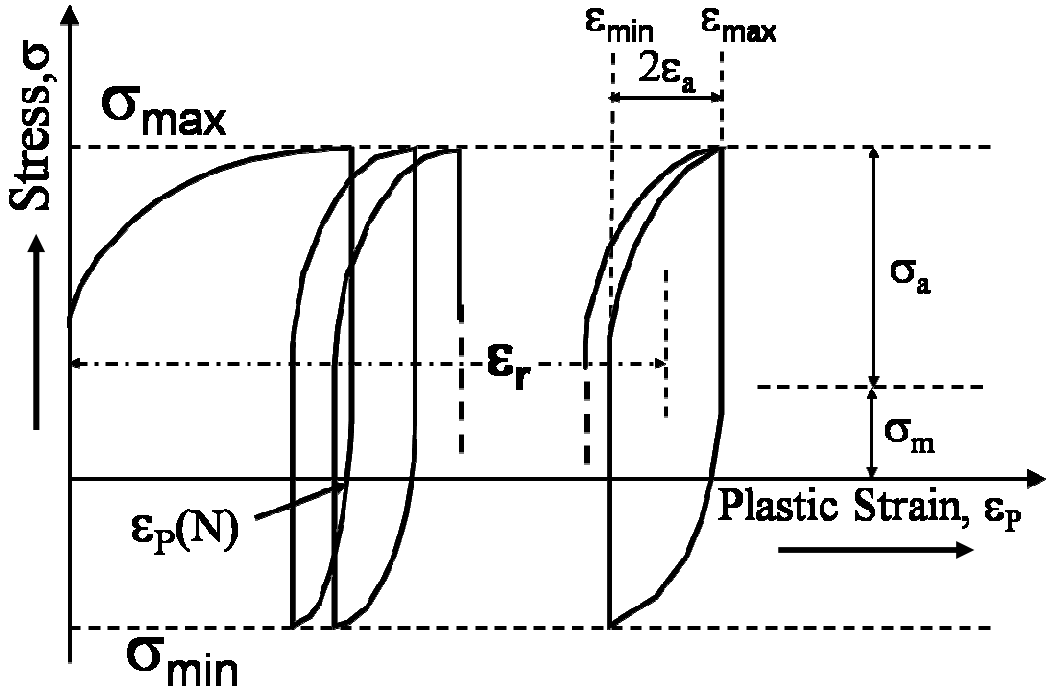

Where,

σ_{max} = Maximum stress σ_{min} = Minimum stress

σ_m = Mean stress σ_a = Stress amplitude

Fig. 2.5: Schematic illustration of ratcheting procedure

Ringsberg has stated that instances where the material shows additional plastic deformation for every load cycle are known as ratcheting [34]. Accumulation of strain continues until the material ductility is exhausted and the material ruptures [34]. The rate of strain accumulation decreases continuously with increase in number of cycles, indicating material response

towards a steady state. Ratcheting strain can be measured numerically as the mean strain for a particular cycle. [7, 10, 19, 24] Ratcheting strain can be expressed as:

$$\varepsilon_r = (\varepsilon_{max} + \varepsilon_{min})/2 \quad (2.7)$$

Where, ε_r = axial ratcheting strain

ε_{max} = maximum strain at a particular cycle

ε_{min} = minimum strain at that cycle.

Ratcheting strain is important in designing and life evaluation of structural components endured in cyclic loading. There are verities of structures that are subjected to cyclic loading where the state of stress exceeds the elastic limit of the materials used. For design and analytic point of view, accurate prediction of ratcheting phenomenon is critical in these types of structures as ratcheting can lead to catastrophic failure. Ratcheting strain (ε_r) increases continuously with number of cycle (N), which shows that there is plastic strain accumulation with time and material fails due to high plastic strain. If ratcheting strain (ε_r) initially increases with the number of cycles (N) and then remains constant, it indicates that there is plastic strain accumulation in the first part of the curve and finally stop in the constant ratcheting strain value region, so material does not fail due to ratcheting. [35]

2.7 Ratcheting: History

Study related to ratcheting behavior of material may be started after the work of Bairstow [5] as mentioned by [3]. This investigation shows the nature of stain accumulation in steel under uniaxial cyclic loading with positive mean stress. At that time the phenomenon was termed as “cyclic strain accumulation”. There came a burst of investigations in the decade of 1950s to understand axial strain accumulation due to uniaxial asymmetric cyclic loading at elevated temperature [36-39] and room temperature [40-42]. Emphasis was given to understand the phenomenon under multiaxial non proportional cyclic loading as reported by Jiang and Sehitoglu [3].

From 1970s onwards investigations were related to the parameters as well as material characteristics which effects ratcheting phenomenon. Material characteristics include cyclic hardening / softening. Lorenzo and Laird [12] have reported comparison of nature of strain accumulations in polycrystalline copper with static creep. They have classified this phenomenon as "cyclic creep acceleration" and "cyclic creep retardation". Interaction of cyclic hardening and cyclic softening behavior was examined by Ruggles and Krempl [43]. Yoshida has reported the effect of stress ratio on ratcheting strain accumulation [17]. Hassan and Kyriakides have worked on ratcheting behavior of cyclically hardenable and softenable materials [19]. Xia et al. have studied the effect of mean stress on ratcheting [44].

From 2000 onwards a lot of works have been done on ratcheting behavior of various materials such as metals, alloys, polymers. Ratcheting and fatigue damage of pressurized pipelines under seismic loading condition has been reported by Van and Mounmi [45]. Uniaxial and multiaxial ratcheting behavior of SS304 at room temperature as well as elevated temperature has been studied by Kang et al. (2002) [18]. Examination of dislocation substructure generation of 316L stainless steel during its room temperature ratcheting experiment has been done by Gaudin and Feaugas [24]. Ratcheting behavior of Pb-Sn solder material has been studied by Chen et al. and Chen et al. [10-11]. Ratcheting behavior of epoxy polymer and its effect on fatigue life has been examined by Tao and Xia [46]. Ratcheting behavior of polymythile methacrylate at various temperatures has been reported by Liu et al. [16]. Ratcheting deformation of super-elastic and shape memory Ni-Ti alloy has been studied by Kang et al. [47].Ratcheting deformations of 304LN stainless steel and interstitial free steel (IF) have been studied by Dutta et al. [26] and Dutta et al. respectively [48].

2.8 Parameters effecting strain accumulation during ratcheting

There are different parameters that effect strain accumulation by ratcheting. Main parameter that effect strain accumulation during asymmetric cyclic loading is types of loading, which indicates how it is applied on the material. Types of loading can be specified as mean stress, stress amplitude, maximum stress, stress rate, stress ratio, cyclic hardening and cyclic softening behavior.

2.8.1 Effect of mean stress and stress amplitude

Several group of researchers [12, 18-20, 49] have reported that strain get accumulated during ratcheting is due to presence of positive or negative mean stress. Earlier investors have reported that accumulation of ratcheting strain decreases with increase in mean stress, which is explained by the graph shown in Figure.2.6, at constant maximum stress condition. It is reported that

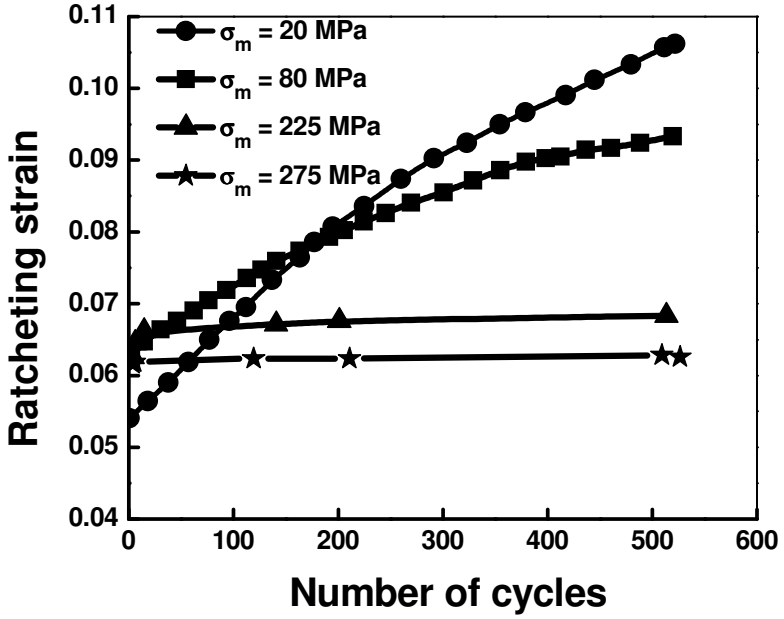

Fig. 2.6: Effect of mean stress on accumulation of ratcheting strain

ratcheting strain and ratcheting strain rate increases with increasing strain level [1]. Strain accumulation due to ratcheting increases with increase in mean stress for lead-tin solder material at constant stress amplitude [11].Researchers have studied the effect of positive to negative mean stress on the nature of strain accumulation of copper alloy and reported that accumulation of strain due to ratcheting positive for positive mean stress and is negative for negative mean stress [13]. Above mentioned investigations of different researchers, reveal that increase or decrease of ratcheting strain depends on the applied mean stress parameter, and also the sign of mean stress.

In case of constant stress amplitude, both ratcheting life and strain accumulation increases with tensile mean stress. In case of tensile and compressive mean stress, strain accumulation paths are mirror of each other. Ratcheting strain amplitude and ratcheting strain rate 63Sn37Pb increases with increase in stress amplitude or mean stress correspondingly [50].

2.8.2 Effect of maximum stress

Maximum stress is an important factor which effect accumulation of strain due to ratcheting. Effect of maximum stress (σ_{max}) on strain accumulation of AISI 316 stainless steel is reported by Feaugas and Gaudin [2]**.** They have reported that accumulation of strain increases with increase in σ_{max} at constant mean stress, which is shown in Figure 2.7. The accumulation of strain value due to ratcheting has been compared with creep strain.

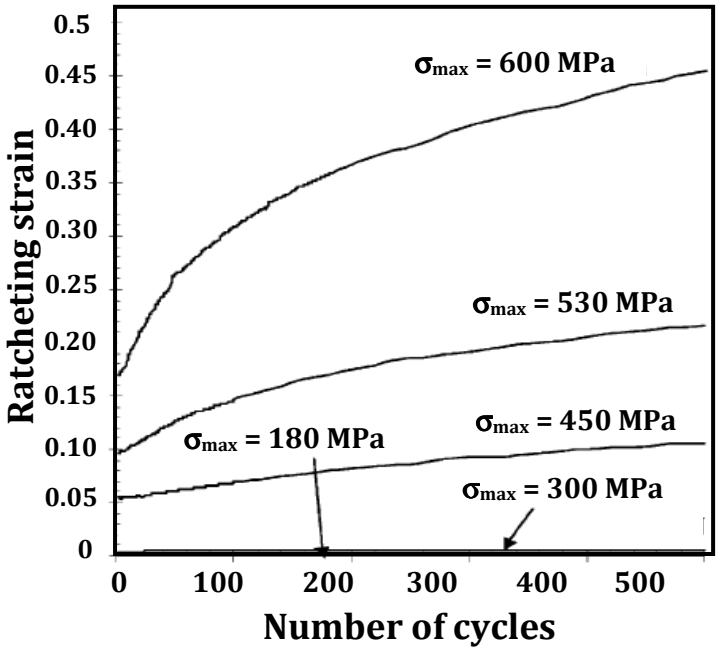

Fig. 2.7: Effect of maximum stress on accumulation of ratcheting

The investigators have reported that in a plot of strain rate ($d\varepsilon/dt$) vs. σ_{max}, there exist two domains. Static creep rate is higher than ratcheting strain rate upto a stress level. This particular stress level is selected as the threshold for ratcheting strain. Below the threshold

level, there is cyclic creep retardation (CCR) zone and above that, cyclic creep acceleration (CCA) zone. These phenomena are illustrated in Figure. 2.8.

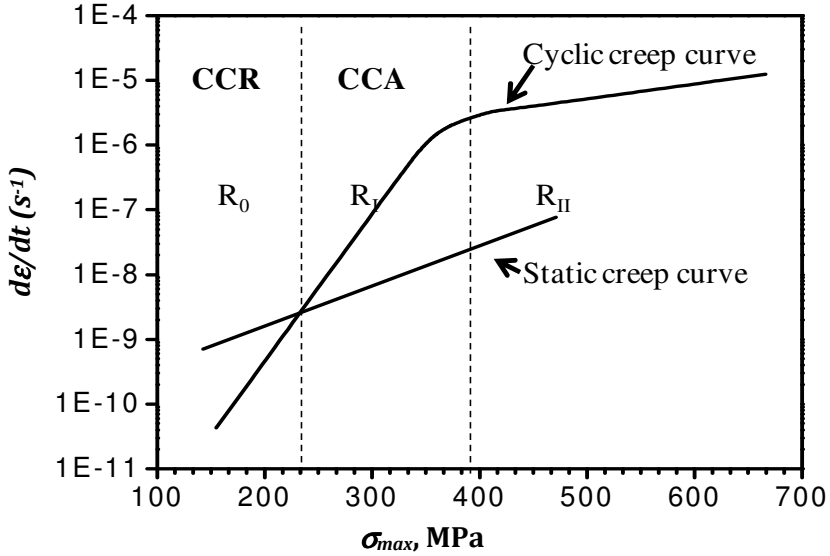

Fig. 2.8: The concept of threshold stress for cyclic creep.

2.8.3 Effect of cyclic hardening and softening features

Ratcheting behavior of the material depends on cyclic hardening/ softening features of the material. Cyclic softening behavior of 25CDV4.11 and cyclic hardening behavior of SS304 stainless steel have been reported by Kang et al.[20]. They have reported that under cyclic softening behavior of 25CDV4.11, ratcheting strain increases with number of cycles.

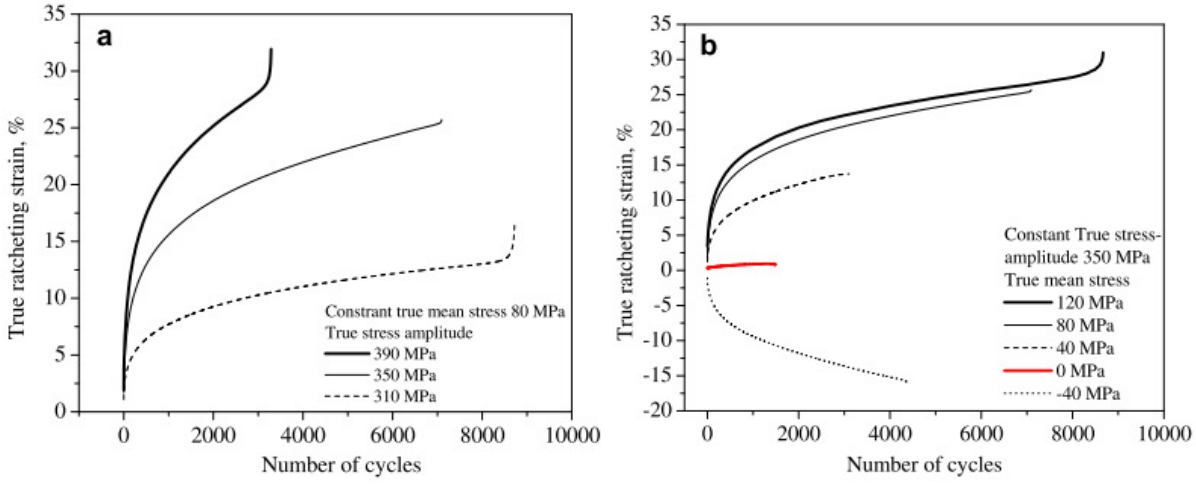

Fig. 2.9: Ratcheting strain *vs.* cyclic number N of (a) 25CDV4.11 steel with load condition of 80 ± 600 MPa. (b) For SS304 with load condition of 65 ± 260

There is no plastic shake down of ratcheting and the material fails due to increase in ratcheting strain. When the material (SS304) is under cyclic hardening behavior, the ratcheting strain decreases with increasing number of cycles. Figure. 2.9 (a) and Figure. 2.9 (b) show Ratcheting strain vs. cyclic number N of 25CDV4.11 steel with load condition of 80 ± 600 MPa. And SS304 with load condition of 65 ± 260 MPa respectively.

2.8.4 Effect of stress ratio

Stress ratio ($R = \sigma_{min}/\sigma_{max}$) acts as an important parameter during asymmetric cyclic loading (ratcheting deformation) of a material. The effect of stress ratio on the nature of the accumulation of ratcheting strain has been reported by a few investigators [9,17]. Yoshida has reported that significant strain accumulation can take place when R is positive or negative. R= -1 is an exceptional case. When R=-1, mean stress is zero, which indicates, symmetric cyclic loading. Hence there is no strain accumulation for R= -1. Plots of ratcheting strain *vs.* number of cycles for various *R* ratios as reported by Yoshida [17] are shown in Figure. 2.10.

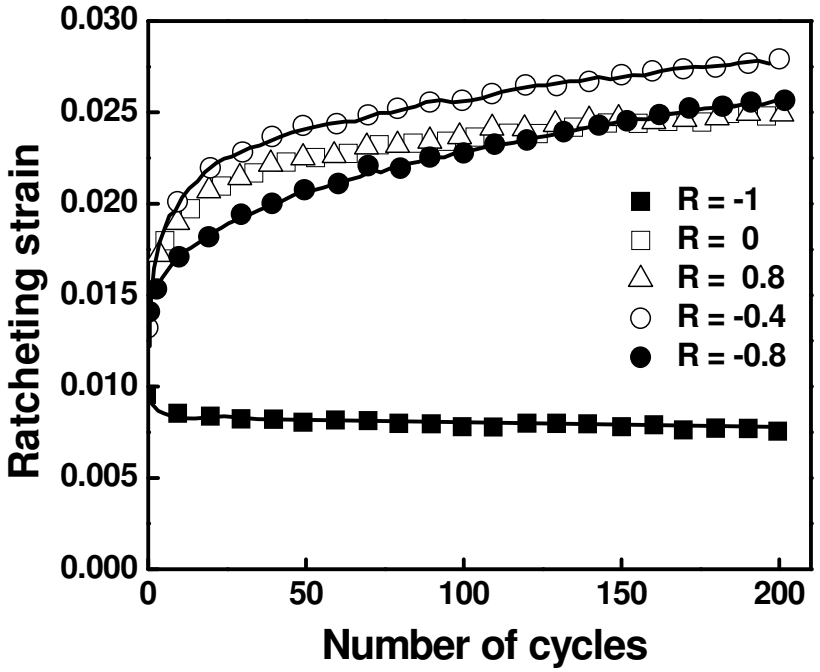

Fig. 2.10: Effect of stress ratio *(*R) on accumulation of ratcheting strain

Results from this figure indicate that strain accumulation due to ratcheting does not increase when *R* increases from 0 to 0.8. Whereas the plot of strain accumulation *vs*. number of cycles for $R = 0.8$ coincides with that for $R = 0$. Gupta et al. have worked on effect of stress ratio on strain accumulation due to ratcheting for SA 333 group 6 piping steel. They have reported that the stress ratio is sufficiently negative for ratcheting to occur.

2.9 Materials on which ratcheting has been studied

There are various material on which ratcheting has been conducted. Ratcheting deformation has been studied for cyclically hardenable material such as SS304, 316L stainless steel and 316FR and cyclically stable such as U71Mn rail steel and ordinary carbon steel [51]. To study the effect of mean stress and ratcheting strain on fatigue life, stress-controlled fatigue tests have been conducted for ASTM A516 Gr 70 steel [52]. C. B. Lim et. al have worked on the ratcheting behavior for copper alloy at room temperature with and without mean stress (σ_m) [13]. The stress controlled fatigue behavior of two dispersion-strengthened aluminum alloys, which are formed by mechanical alloying, is examined. The results of plastic strain-controlled LCF tests for a conventional A1-Mg alloy (AA5083-H321) are compared with conventional precipitation-strengthened alloy (AA7075-T6) [53].The understand the effect of annealing treatment on ratcheting behavior and its associated microstructure and also monotonic tensile properties is assessed for extruded AZ31B magnesium alloy [54]. There are several factors, which effect ratcheting behavior. Uniaxial ratcheting behavior of 63Sn/37Pb is carried out at room temperature under different loading conditions [50]. To study the effect of σ_a, σ_m, and loading history and stress ratio on the ratcheting behavior, high-nitrogen steel was subjected to cyclic loading. [55]. Microscopically ratcheting behavior is related to the mobility of dislocations during the cyclic loading. It is supposed that the metals having different crystal structure or value of different stacking fault energy may show more or less different ratcheting behaviors [56]. The hysteresis loops are almost symmetrical with respect to both the stress and strain axes for materials having high stacking fault energy. On the other hand, the loops are always displaced with respect to the strain axis in the direction of the first applied stress for materials having low stacking fault energy [56,57]. The fatigue failure process attacks the weakest links within the test material, which act as nucleation sites for crack origin [58].

2.10 Deformation induced martensite and quantitative estimation of volume fractions

It is well known that the structures of austenitic stainless steels are metastable upon deformation and austenitic phase transforms to martensite. Such a type of transformation during plastic deformation provides a desirable combination of strength and toughness to austenitic stainless steels. In general, martensitic transformation is believed to be triggered when the austenitic stainless steel is deformed at temperatures below M_d, a temperature below which the transformation to martensite readily takes place [59, 60]. In fact, a number of investigations [61-64] have been carried out to understand the martensitic transformation in metastable systems. Critical review of these investigations leads to infer that the nature of such phase transformation is associated with the chemical composition of the material, rate of deformation, total strain, stress state and temperature of deformation [61, 65, and 66]. Considerable database is available on this topic for austenitic stainless steels in general, for tensile deformation of the steel, and a few reports exist for cyclic deformation. Whereas, studies related to phase transformation during ratcheting deformation are a few. Hence, investigations are necessary to understand to the deformation induced phase transformation in stainless steel during ratcheting deformation. The quantitative estimation of deformed phases has been done by De et al. [67] for tensile deformation; the method is described below.

X-ray diffraction analysis is required for this type of quantification, from which it can be stated that total integrated intensity of all diffraction peaks for each phase is proportional to its volume fraction. It can be stated that [67]:

$$I_i^{hkl}=CR_i^{hkl}V_i/2\mu \qquad (2.8)$$

Where,

$$C=\left(\frac{I_0 A\lambda^3}{32\pi r}\right)\left[\left(\frac{\mu_0}{4\pi}\right)\frac{e^4}{m^2}\right] \quad \text{and,}$$

$$R_{hkl}=\left(\frac{1}{v^2}\right)\left[|F|^2\ p\left(\frac{1+\cos^2 2\theta}{\sin^2\theta\cos\theta}\right)\right]\left(e^{-2M}\right)$$

In the mentioned equations,

I_i^{hkl}: integrated intensity for (hkl) plane of i-phase, i: γ, α;

C: the instrument factor;

R_i^{hkl} is the material scattering factor and depends on diffraction angle (θ), interplanar spacing of hkl, composition and crystal structure of phase i;

υ is the volume of unit cell,

$F_{hkl}$is the structure factor for reflecting phase (hkl),

The structure factoris independent of the shape and size of the unit cell.

p: multiplicity factor,

It can be defined as the number of different planes in a form having the same spacing. Parallel planes with different Miller indices, such as(100) and (-100), are counted separately as different planes, yielding numbers which are double those given in the preceding paragraph. Thus the multiplicity factor for the {100} planes of a cubic crystal is 6 and for the {111} planes 8.

e^{-2M}: temperature factor

The intensity of a diffracted beam decreases as the temperature is raised, and, for a constant temperature, thermal vibration causes a greater decrease in the reflected intensity at high angles than at low angles.

λ: the wavelength of incident X-ray beam,

μ: linear absorption coefficient,

A: cross sectional area of incident X-ray beam,

I_0 : intensity of the incident beam,

r: radius of diffractometer circle,

e, m: charge and mass of electron.

Therefore, for a steel containing austenite (γ), bcc martensite (α') and hcp-martensite (ε), then Eq. (1) may be written as:

$I_\gamma = K R_\gamma V_\gamma / 2\mu$ and

$I_{\alpha'} = K R_{\alpha'} V_{\alpha'} / 2\mu$

Additionally,

$$V\gamma + V\alpha' = 1 \qquad (2.9)$$

From the above relations, and knowing that C/2μ is constant in a given X-ray diffraction scan, the volume fraction of austenite and martensite can be derived for numerous peaks as [68]:

$$V_i = \frac{\frac{1}{n}\sum_{j=1}^{n}\frac{I_i^j}{R_i^j}}{\frac{1}{n}\sum_{j=1}^{n}\frac{I_\gamma^j}{R_\gamma^j} + \frac{1}{n}\sum_{j=1}^{n}\frac{I_{\alpha'}^j}{R_{\alpha'}^j}} \qquad (2.10)$$

Where,

i = γ, or α' in this instance and n is the number of peaks examined.

Eq. (2.10) enables simultaneous calculation of the volume fraction of austenite and α'-martensite in non-conventional stainless steel from a single XRD scan.

CHAPTER 3

EXPERIMENTAL

Experimental

3.1 Introduction

The aim of this investigation is to study the cyclic deformation behavior of a non-conventional austenitic stainless steel, in conjugation with the investigations related to deformation induced phase transformation. To fulfill these aims, different kinds of experiments were conducted which are described in this chapter. An overview of all the experiments includes determination of chemical composition of the selected steel, heat treatment, microstructural characterization, determination of tensile behavior of the steel, study of facture surfaces, experiments related to stress-controlled asymmetric fatigue behavior, X-ray diffraction studies, scanning electron microscopy and pre and post-fatigue hardness tests.

3.2 Material Selection

A non-conventional special grade austenitic stainless steel which is known as X12CrMnNiN17-7-5 according to ISO/TR 15510:1997 [65] was selected for this investigation. This material is commercially pure in nature. It was available in the form of rod with diameter 16 mm.

3.3 Chemical composition

The chemical composition of the selected steel was assessed using optical emission spectrometer (model: ARL 3460 Metals Analyzer, Thermo Electron Corporation Limited, Switzerland).

3.4 Heat Treatment

The selected material was procured from market for which the pre-deformation history is not known. Therefore, it is required to remove any residual stresses that may present in it. Further, heat treat of stainless steel involves solution annealing, which helps in dissolving any precipitated carbide phase at high temperature. The precipitated carbides may cause lesser corrosion resistance. Solution treatment of the investigated stainless steel was done by heating the steel at 960°C for 1 hour which was followed by water quenching.

3.5 Metallography

For microstructural studies, samples of approximately 10 mm height were cut from the heat treated rods. Samples were ground roughly on a belt grinder. Grinding was done by moving the samples up and back across the surface of the flat belt grinder. During grinding operation samples were kept cool by repeated dropping into water. After rough grinding, samples were polished by a series of emery papers. Emery papers contain consecutively finer abrasive grains such as grades of 1/0, 2/0, 3/0 and at last 4/0. The samples were moved in perpendicular direction to the existing scratches during each polishing operation.

After polishing through the series of emery papers samples were polished by using wet rotating wheel covered with special cloth that was charged with abrasive. Process of polishing was continued until the surface is plane and free of nicks or inflection etc. After polishing samples were carefully cleaned with soap solution, and subsequently dried using drier. These samples were then polished using diamond paste up to 0.25 mm surface finish. In addition to that, the samples were electro polished using a solution of 20% perchloric acid and 80% acetic acid in ice-cooled atmosphere. The polished specimens were etched with aqua regia solution [75%HCl and 25% HNO_3].

3.5.1 Optical Microscopy

Microstructure of the samples were obtained by optical microscope (Model: Olympus BX61, Tokyo, Japan), and images were captured at different magnifications. Optical microscope has been shown in Figure 3.1.

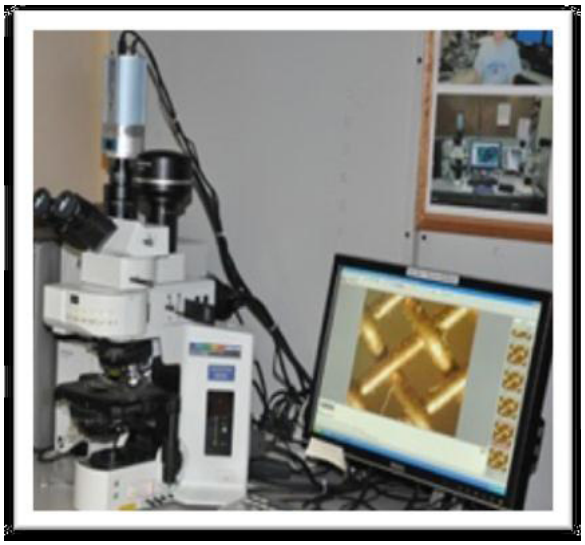

Fig3.1: Image of optical microscope

3.5.2 Grain size Measurement

The average grain size of the investigated steel was determined with the help of liner intercept method according to ASTM standard E-112 [69]. As per the method, a liner test grid was superimposed on a typical microstructure. Number of stainless steel grains intercepted by the test lines was counted. Such measurements were repeated on 10 randomly chosen fields at a magnification of 200X. The average grain size was anticipated by using the formula

$$d = L_T/N_L \quad (3.1)$$

Where

N_L = Number of grains intercepted by a unit true test line length.

L_T = True length of the test line.

True length of the test line can be defined as the length of the test line at unit magnification.

3.5.3 Hardness Determination

Hardness tests were done by using a Vickers Microhardness Tester (Model: Leco LV 700, USA); the machine is shown in Figure 3.2. To ensure accuracy of measurement, samples were ground flat and parallel to opposite surfaces using belt grinder; followed by mechanical polishing of the sample following the procedures mentioned in section 3.4.

Fig.3.2: Leco LV 700 Vickers Microhardness

Hardness tests were done by using an indentation load of 5gf. To obtain average hardness at least 3 readings were considered for each sample. Vickers hardness was calculated by using the relations:

$$H_V = 1.854P / (d_{avg})^2 \qquad (3.2)$$

Where

P= applied load in kgf.

$d_{avg} = (d_1+d_2)/2$

Where, d_1 and d_2 are the lengths of two indentation diagonals.

3.6 Mechanical Testing

3.6.1 Tensile properties determination

Tensile tests were carried out at room temperature (300K) on the cylindrical specimens having gauge length of 25 mm and diameter of 6 mm. These specimens were fabricated from heat treated cylindrical rods of 120 mm initial length and 16 mm initial diameter according to ASTM standard E-8M [70]. For tensile test specimens were polished in lathe machine up to fine polishing. All tensile tests were carried out using a servo-hydraulic INSTRON (8800R, Birminghamshire, UK) testing machine, at a constant cross head speed of 1mm/ min. This cross head speed corresponds to nominal strain rate of 6.66×10^{-4} s^{-1}. For each test load, displacement signals were automatically recorded, and the digital values of load and displacement were stored in a computer for subsequent processing.

3.6.2 Fatigue properties of material

Stress controlled fatigue experiments were carried out at room temperature (300K) using servo-hydraulic universal testing machine (Model: INSTRON, 8800R).

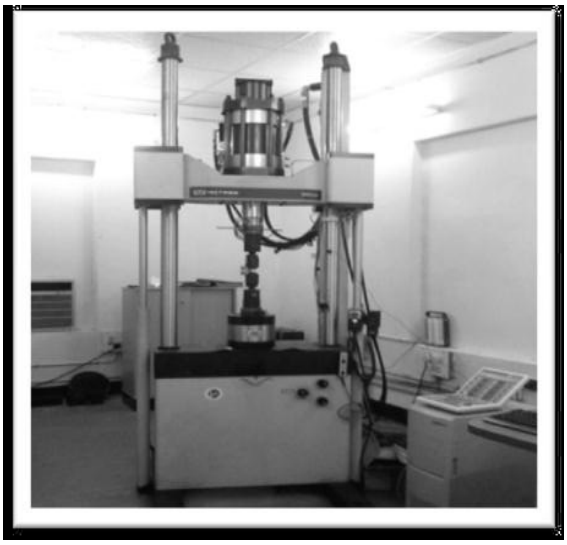

Fig.3.3: Servo hydraulic INSTRON 8800R machine

The specimens used for fatigue studies were similar to those used for tensile testing only with the variation that the fatigue specimens were of 7 mm diameter.

All tests and data acquisitions were done in stress control mode at constant stress rate of 50Mpa/S. The variables that have been considered for this test are mean (σ_m) stress and stress

amplitude (σ_a) and number of cycles. These test parameters were chosen in such a way that these can be classified into two categories (i) constant σ_m with varying σ_a (ii) constant σ_a with varying σ_m. All these details are listed in Table 3.1. During each test, the load- extension as well as the actuator displacement data was continuously recorded by using the attached software to the computer. It was aimed to acquire at least 200 data points per cycle during

Table1. Test Matrix for Ratcheting Test

Material	**Sl No.**	**σ_m (MPa)**	**σ_a (MPa)**
A Non Conventional Stainless steel	1	100	400,450,500
	2	150	400,450,500
	3	200	400,450,500

fatigue tests. All fatigue tests were done upto 50 and 100 cycles for further analysis on these samples. Figure 3.3 shows servo hydraulic INSTRON 8800R machine.

3.7 Factography

To study the fracture surface, transverse sections from the gauge potion of the broken tensile samples were cut. Fracture surface of the samples were taken by scanning electron microscope (SEM) at different magnifications.

Fig.3.4: Scanning electron microscopy.

3.8 X-ray Diffraction and Scanning Electron Microscopy

To investigate the possible structural alternations during tensile and fatigue loading, tensile/cyclically deformed specimens were cut and these were subjected to X-ray diffraction (XRD) and scanning electron microscopy (SEM) analyses(Model: JEOL-JSM 6480LV). SEM was operated at a voltage of 20 KV. Scanning electron microscope is shown in Figure 3.4. The XRD (Model: XPert-3040Y00, Holland) analyses were carried out using high resolution Cu-Kα radiation. Samples were subjected to XRD in the scanning range of 20°-120° and scanning rate of 2°/min.

3.9 Post-ratcheting Hardness

For post-ratcheting hardness determination, transverse sections of the gauge portion of the ratcheted samples were cut with approximate height of 8 mm, after cutting the portion containing the fracture surface. Specimens were prepared for hardness studies as mentioned in Section 3.4.3.

CHAPTER 4
RESULTS AND DISCUSSION

Results and Discussion

4.1 Introduction

The aim of this investigation is to study the low cycle fatigue (LCF) behavior of a non-conventional stainless steel particularly under stress-controlled asymmetric cyclic loading conditions. It was also intended to determine possible in situ phase transformation of the investigated steel during ratcheting deformation, as it is known that austenitic stainless steel is metastable up on deformation. To fulfill these aims various experiments have been conducted, which are described in chapter 3. This chapter deals with the obtained results of all the experiments conducted during this investigation in association to their pertinent discussion. The chapter is divided into various sub-sections: **Section 4.1** deals with chemical composition of the investigated steel; microstructural analyses have been discussed in **Section 4.2**; results of conventional mechanical properties have been provided in **Section 4.3** with relevant discussion, **Sections 4.4** to **4.6** includes results and discussion of uniaxial ratcheting deformation, in-situ variation of microstructure, fractographic features of the broken tensile sample and post fatigue hardness variations respectively.

4.2 Chemical composition

Chemical composition of the investigated special grade non-conventional stainless steel (X12CrMnNiN17-7-5) was obtained by OES, which is shown in table 4.1. This grade of stainless steel is analogous to X5CrNi17-7 [68]. X12CrMnNiN17-7-5 stainless steel has good mechanical properties and good corrosion resistance. This grade of steel are mostly used for automotive parts such as automotive trim, automotive wheel covers and also use in flat conveyor chains, flatware, railroad passenger car bodies, structural members and architectural applications. It is known that austenitic stainless steels possess major alloying elements as Cr and Ni approximately in the range of 16-25% and 8-20% respectively with low carbon content [71]. The investigated stainless steel is having 0.14% carbon with common alloying elements of Ni and Cr as

Table 4.1: Chemical composition of the non-conventional stainless steel (all in wt. %).

Material	Elements						
ISO/TR 15510 X12CrMnNiN17-7-5 SS	**C**	**Ni**	**Cr**	**Mn**	**Al**	**Ti**	**V**
	0.14	3.96	15.6	5.49	0.03	0.02	0.06
	Si	**S**	**P**	**Mo**	**Cu**	**N**	**Fe**
	0.53	0.016	0.042	0.2	1.05	0.135	Bal

3.66% and 15.6% respectively. The steel also contains 5.49% Mn. Manganese is added to this special grade of steel in order to conserve Ni. As the alloying elements are different as compared to that in conventional 300 series austenitic stainless steel, this steel is referred to as non-conventional austenitic stainless steel [68]. It is known that Ni, Mn and N are austenite stabilizers and hence this steel is austenitic at room temperature; thus the crystal structure of the steel is *fcc*.

4.3 Microstructural analysis

Optical microstructure of the investigated non-conventional stainless steel reveals that the steel possesses equiaxed austenite grains. Optical micrographs of the non-conventional stainless steel were taken at various magnifications. A typical micrograph of the investigated stainless steel is shown in figure 4.1. Grain size is obtained by using linear intercept method according to ASTM standard E112 [69]. Average grain size of the specimen was found to be 23.79±3.6 µm.

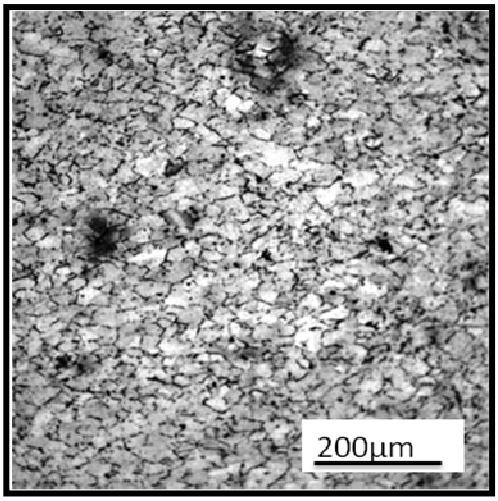

Fig.4.1: A typical micrograph of investigated stainless steel.

4.4 Conventional mechanical properties

Investigated conventional mechanical properties of the stainless steel include hardness and tensile properties. Microhardness tests of the specimen were carried out using Vickers microhardness tester and tensile tests were done by servo-hydraulic universal testing machine (Model: INSTRON, 8800R).

4.4.1 Hardness determination

Microhardness of the non-conventional stainless steel was taken at different positions of the sample. At least three readings were taken for each sample to obtain average value of hardness. The results are listed in table 4.2.

Table 4.2: Microhardness values of the non-conventional stainless steel

Material	D_1 (µm)	D_2 (µm)	$Hv_{0.050}$	Average $Hv_{0.050}$
ISO/TR 15510 X12CrMnNiN17-7-5 SS	21.08	20.98	209.7	213.86
	20.27	21.25	215.1	
	20.26	21.10	216.8	

Dwell time for microhardness test is 15 sec, with applied load of 5gf. As per literature, austenitic stainless steels possess hardness ≈ 200 VHN [73]. Current results indicate that the hardness of the investigated steel is 213.86 $Hv_{0.050}$. From Table 4.2 it is clear that hardness of the investigated stainless steel falls under the hardness range of austenitic stainless steel.

4.4.2 Tensile properties

Load and elongation values were obtained from the servo-hydraulic universal testing machine. Corresponding stress and strain values for the load and elongation is calculated and plotted to get stress vs. strain curve. Tensile parameters are yield strength and ultimate tensile strength. The tensile stress-strain curves were obtained at room temperature. Average tensile properties of the steel were obtained from two experiments. Figure 4.2 (a) shows the engineering stress-strain curve of the investigated non-conventional stainless steel with strain rate of 1.33×10^{-3} s^{-1}. Engineering stress-strain plot of the investigated stainless steel shows continuous yielding behavior.

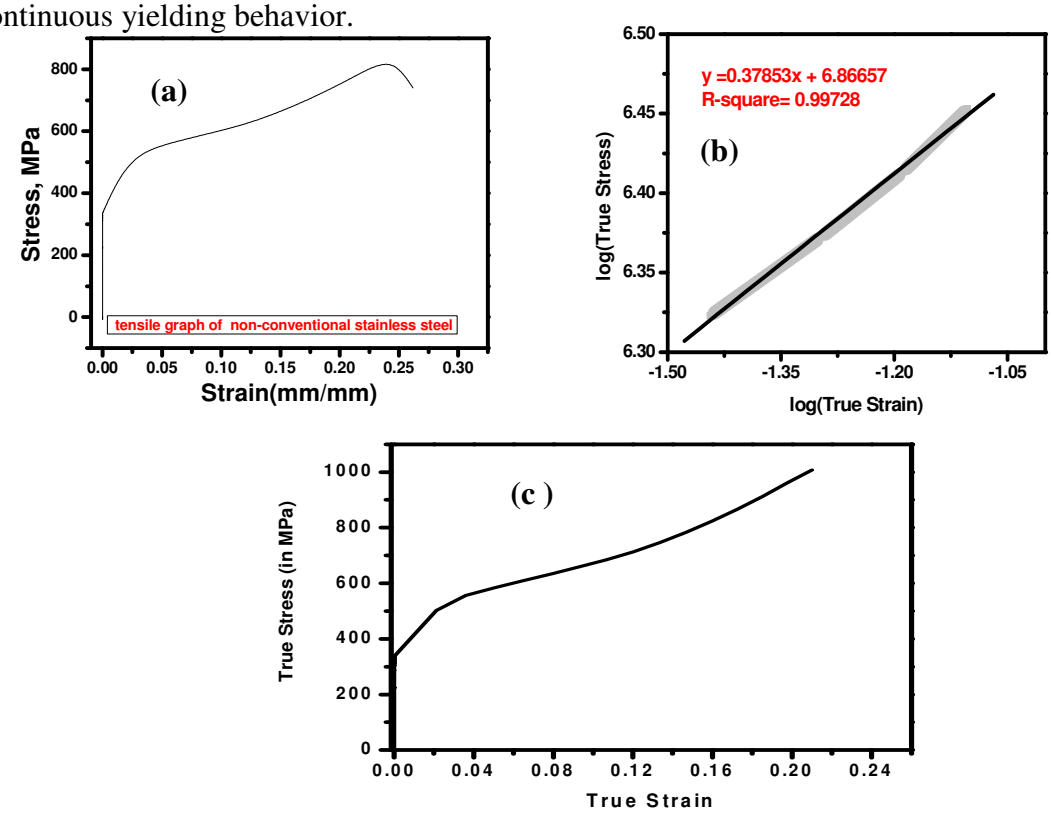

Fig.4.2: a) Engineering stress strain curve of the investigated stainless steel (b) Log (true stress) vs. log (true strain) in the plastic domain (c) True stress-strain plot of the investigated stainless steel

Therefore, 0.2% strain offset procedure (as suggested in ASTM standard E8M) [70] has been used to determine its yield strength. Tensile results are tabulated in table 4.3. To estimate the strain hardening exponent (n) of the investigated material, true stress (σ) and true strain (ε) values are calculated from the data of engineering stress and engineering strain. The obtained results are plotted as log (true stress) vs. log (true strain) in the plastic domain which results in to straight line as shown in Figure 4.2(b). True stress-strain plot of the investigated steel is shown in figure 4.2 (c). Strain hardening exponent values are calculated using Hollomon equation $\sigma=K\varepsilon^n$, where K is strength coefficient [28]. The values of n have been estimated from the log-log plot, where as strength coefficient is calculated from the intercept of this plot to the stress axis at ε=1). Here the strain hardening coefficient was found to be 0.38 in the strain range of 4%-8% used. The obtained result of strain hardening exponent is in good agreement with that reported by Dutta [26] for AISI 304LN stainless steel.

Table 4.3: Tensile properties of the investigated stainless steel.

Material	Yield Strength (MPa)	Tensile strength (MPa)	Uniform elongation % (e_u)	Total elongation % (e_t)
ISO/TR 15510 X12CrMnNiN17-7-5 SS	485	826.4	23	26

After tensile tests, the broken tensile specimens have been subjected to scanning electron microscopy for observation of the fracture surface. A typical factograph is shown in Figure 4.3. This reveals dimple morphology, as can be expected for a ductile material like stainless steel. It is known that the mechanism of ductile fracture is constituted of three successive events; such as void nucleation, growth and their coalescences [72-76]. On analyzing all the fracture surfaces it is concluded that the nucleation of voids in ISO/TR 15510 X12CrMnNiN17-7-5 stainless steel is created by dislocation-dislocation interaction. Fracture surface of the investigated stainless steel reveals that fracture surface consists of different sizes of dimples at different places. This fact indicates that a few voids have grown substantially during fracture.

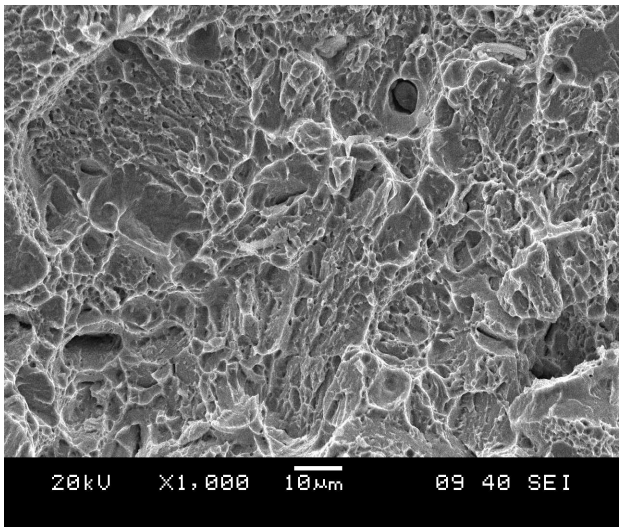

Fig.4.3: Atypical factograph of the broken tensile specimen.

4.5 Uniaxial ratcheting behavior

The results of ratcheting tests conducted up to 50 and 100 cycles under different combinations of mean stress and stress amplitude have been incorporated and subsequently discussed in this section. It is reported in literature that accumulation of ratcheting strain attains a saturation plateau after 100 cycles of loading for stainless steel [77]. Therefore, a part of all ratcheting tests conducted in this investigation have been done up to 100 cycles. Another series of tests have been done up to 50 cycles for comparison. In this investigation uniaxial ratcheting behavior has been observed at constant mean stress (σ_m) with varying stress amplitudes (σ_a) and at constant stress amplitude with varying mean stress values.

4.5.1 Nature of hysteresis loops

Cyclic stress-strain hysteresis loops were generated from the uniaxial ratcheting experiments on the investigated material under different positive mean stress values. It is known that asymmetric cyclic loading with non-zero mean stress produces unclosed hysteresis loops [48]. This fact can be observed from the shifting of hysteresis loops and thus it can be understood that strain is continuously getting accumulated with cycles.

Typical hysteresis loops those were generated during stress-controlled asymmetric cyclic loadings with σ_m- σ_a combinations of 200 MPa - 400 MPa and 200 MPa - 500 MPa are presented in Figure 4.4 and 4.5 respectively. Hysteresis loops of first and second cycles for σ_m = 200 MPa and σ_a = 400 MPa is being shown in Figure 4.4 (a), where points R and S represent the maximum and minimum strain for the second cycle. Average of maximum and minimum strain in a particular cycle is taken as strain accumulation in that cycle.

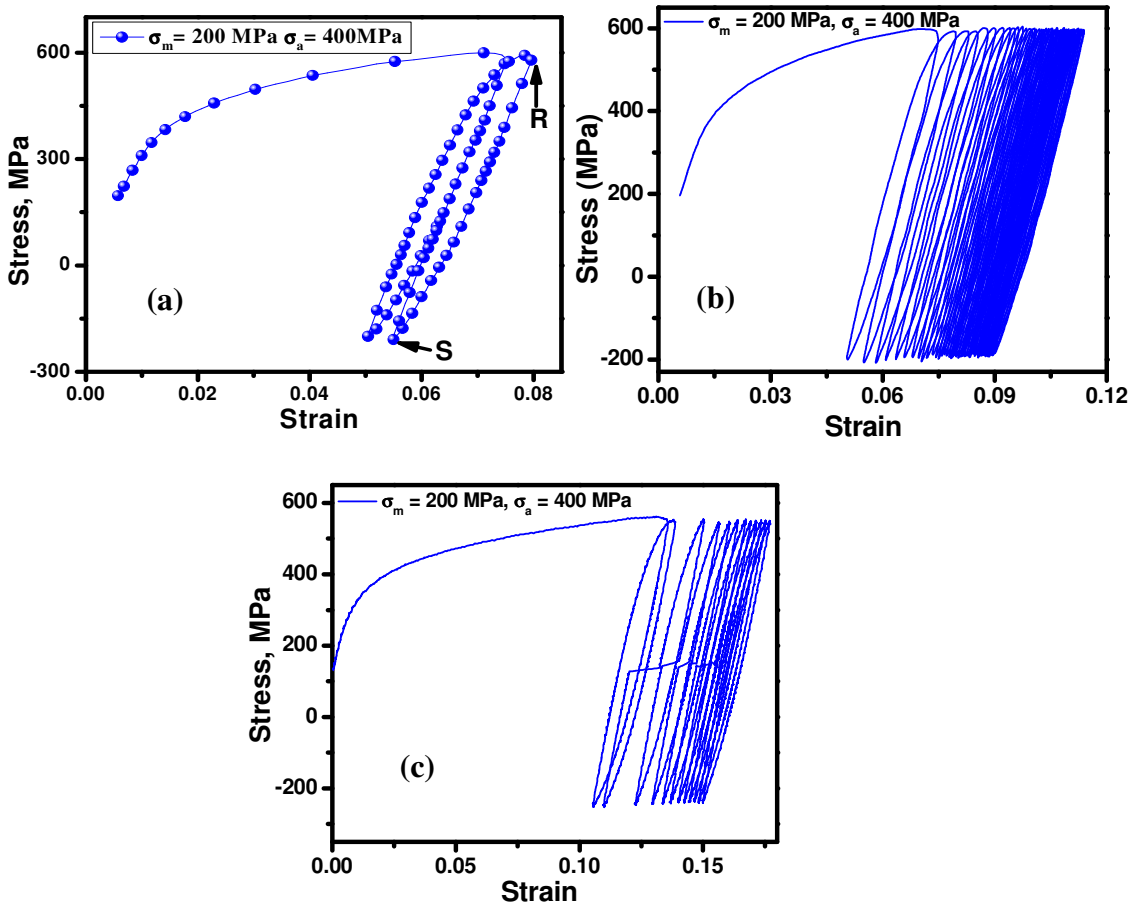

Fig.4.4: Hysteresis loop (a)For first and second cycle (b) For 50 cycles (c) For 100 cycles at σ_m = 200 MPa, σ_a = 400 MPa.

Figure 4.4 (b) and Figure (c) shows hysteresis loops for 50cycles and 100 cycles respectively and the graphs show that hysteresis loops are being shifted towards more strain direction during ratcheting deformation, which in turns induce more plastic strain to the material. Hysteresis loop of first cycles for σ_m = 200 MPa, σ_a =500 MPa is shown in Figure 4.5 (a). Figure 4.5(b) and Figure4.5 (c) shows hysteresis loops of 50 and 100 cycles for σ_m =200

MPa, σ_a = 500 MPa respectively. Strain accumulation is quite more in second case, which is discussed in the upcoming sections.

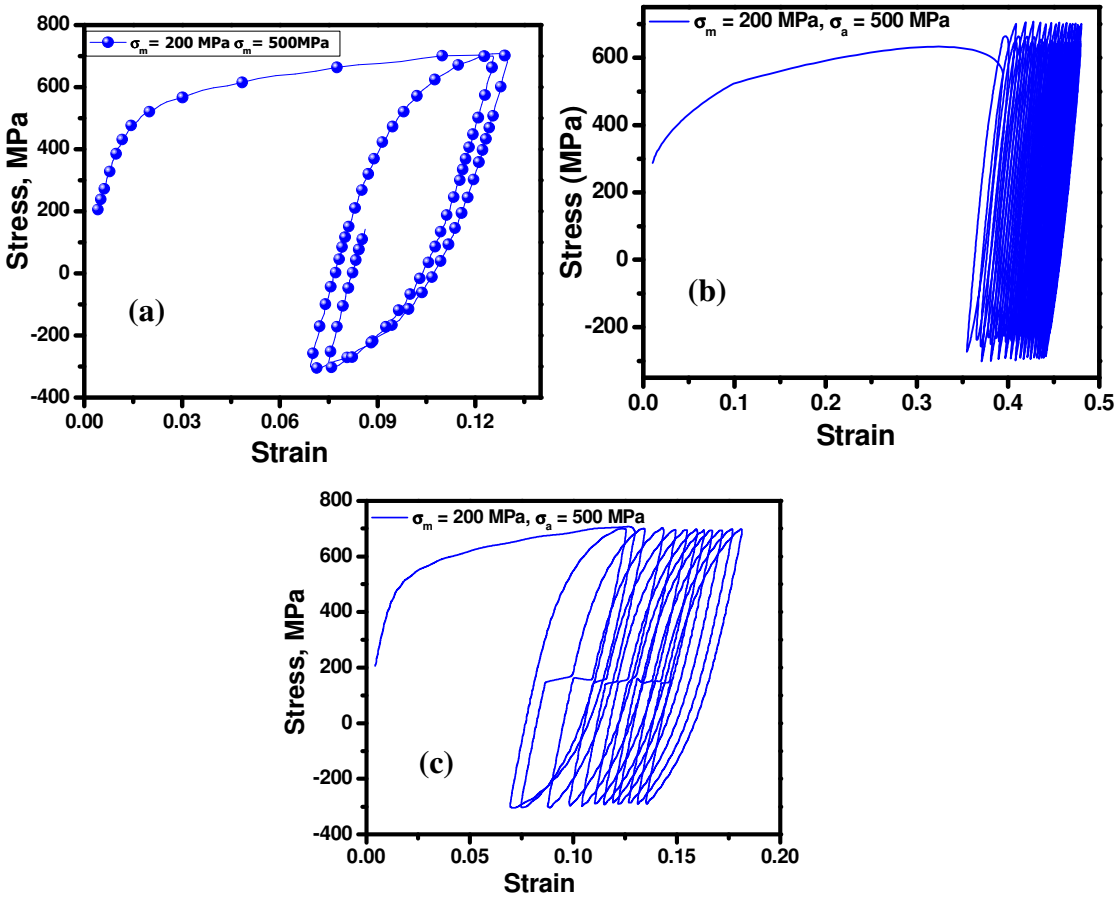

Fig.4.5: Hysteresis loop (a)For first and second cycle (b) for 50 cycles (c) For 100 cycles at σ_m = 200 MPa, σ_a = 500 MPa.

4.5.2 Strain accumulation: Effect of mean stress at constant stress amplitude

Figure 4.6 and Figure 4.8 illustrate the effect of σ_m on accumulation of ratcheting strain (ε_r) for 50 cycles and 100 cycles. Variation in accumulation of ratcheting strain of the investigated non-conventional stainless steel under asymmetric cyclic loading for the condition of varying mean stress of 150, 200 MPa with constant stress amplitude of 400 MPa is shown in Figure 4.6 (a). Similar plots are shown in Figure 4.6 (b) and Figure 4.6 (c) for σ_a = 450 MPa and 500 MPa respectively. These graphs show that strain accumulation increases with increase in

mean stress. For σ_m=150 MPa and σ_a= 400 MPa strain accumulation is 8.78%. For σ_m - σ_a combination of 200 MPa – 400 MPa strain accumulation is 14.47%. Strain accumulations are 10.16 %, 14.65 %, 30.89 % and 46.20 % for σ_m = 150 MPa with σ_a = 450 MPa, σ_m = 200 MPa with σ_a = 450 MPa, σ_m = 150 MPa with σ_a = 500 MPa and σ_m = 200 MPa with σ_a = 500 MPa respectively. Increase of ε_r with increasing σ_m level of 150, 200 MPa at constant σ_a = 500 MPa is explained by histogram shown in Figure 4.6 (d).

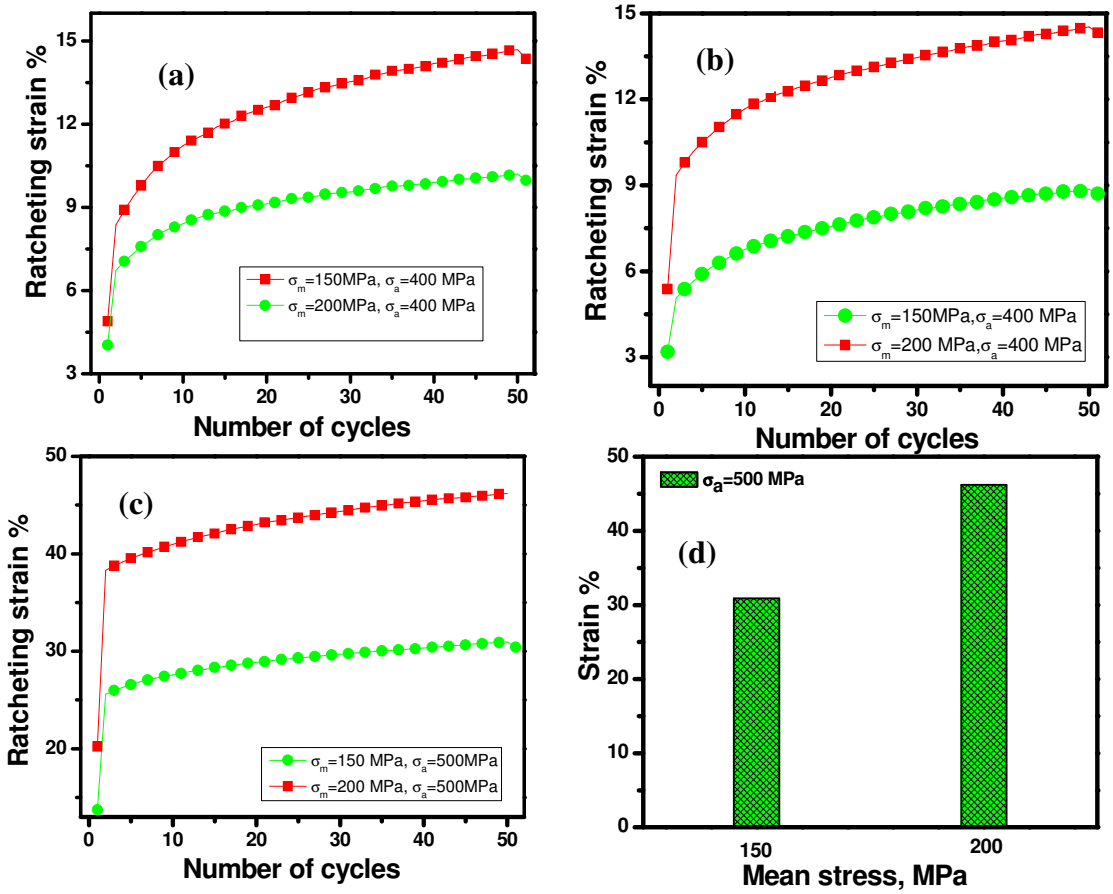

Fig .4.6: Variations of ε_r with number of cycles for (a) σ_m (150,200MPa) at constant σ_a (400 Mpa) (b) (150,200 MPa) at constant σ_a (450MPa) (c) (150, 200 MPa) at constant σ_a (500 MPa) after 50cycles (d) Histogram showing the variation of ε_r for σ_m (150,200MPa) at constant σa (500 Mpa).

To explain the increase in strain accumulation with increase in mean stress, a schematic diagram of shifting of hysteresis loop is shown in Figure 4.7 (a) at constant σ_a. σ_m is lower in case I as compare to case II. With increase in σ_m both maximum and minimum stress increase, which results in shifting of hysteresis loops in upward direction. To compare it with actual case, let us consider typical cases. Figure 4.7 (b) shows shifting of hysteresis loops of constant stress amplitude of 500 MPa with increasing mean stresses 150 MPa and 200 MPa. In case of σ_m =150MPa with σ_a = 500 MPa, maximum and minimum stress are 650 MPa and -350 MPa respectively. With increase in mean stress σ_m =200 MPa with σ_a = 500 MPa there are increase in maximum and minimum stress values of 700 MPa and -300 MPa respectively.

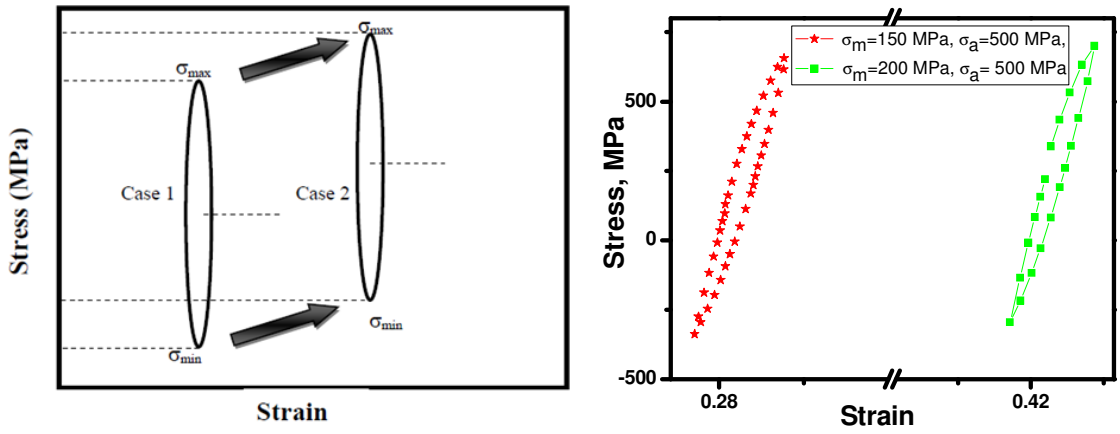

Fig.4.7: (a) Schematic diagram of shifting of hysteresis loop (b) Shifting of hysteresis loop of varying σ_m (150, 200 MPa) at constant σ_a (500 MPa).

According to Ray et.al [77] this fact causes increasing amount of dislocation generation, when mean stress is increased to a higher level. The increase in strain accumulation with increasing mean stress can be described as a consequence of increasing dislocation density, at higher mean stress levels. As cyclic loading during ratcheting deformation is asymmetric in nature, number of dislocations those generate during forward loading, does not get annihilated during backward loading sequence and thus significant amount of dislocations remains in the structure which causes increased dislocation density. Although some transmission election microscopy may reveal this fact more accurately, this could not be done during the current investigation.

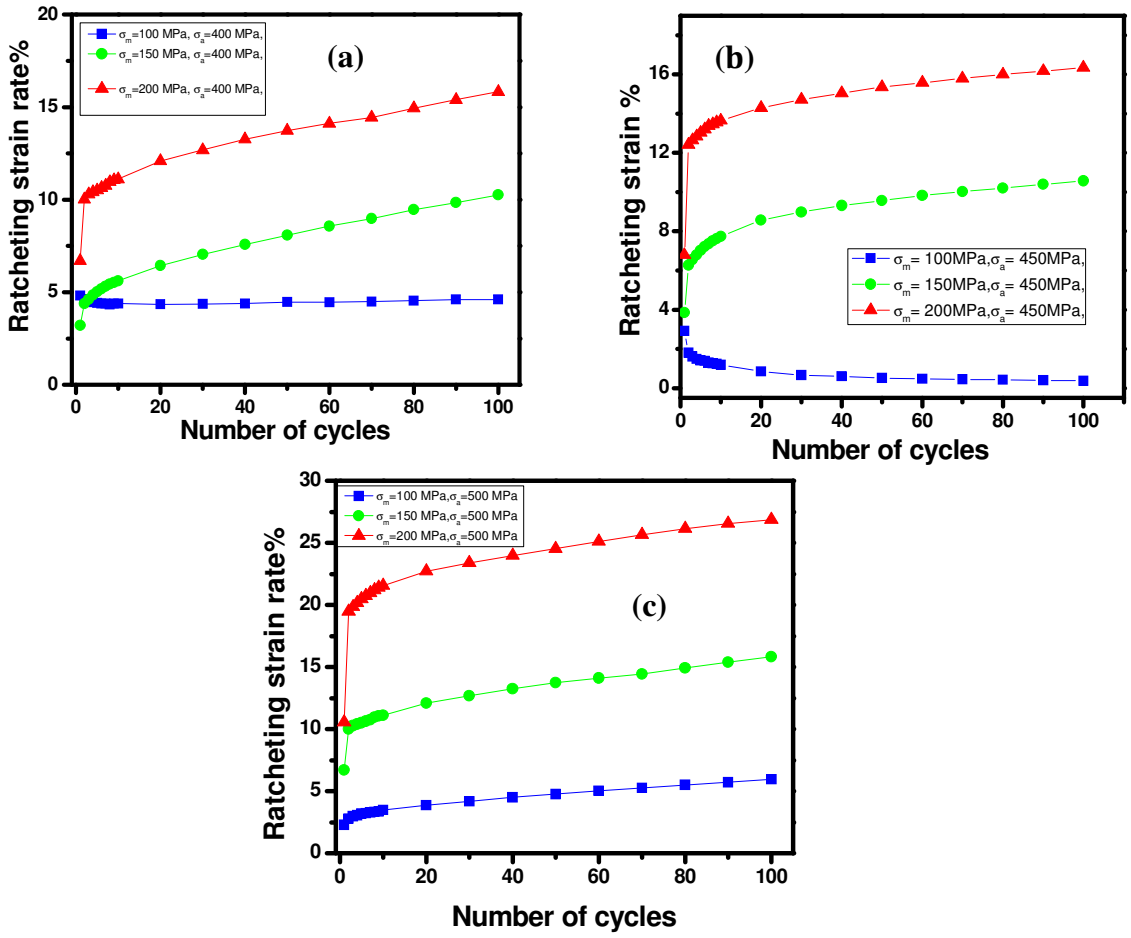

Fig .4.8: Variations of ε_r with number of cycles for (a) σ_m (100,150 and 200 MPa) at constant σ_a (400 MPa) (b) σ_m (100,150,200 MPa) at constant σ_a (450 MPa) (c) σ_m (100,150 and 200 MPa) at constant σ_a (500 MPa) after 100 cycles.

Figure 4.8 illustrates the effect of σ_m at constant σ_a level of 400MPa and 450 MPa on ε_r for 100 cycles respectively. Figure 4.8 (a) illustrate the effect of σ_m (100,150,200 MPa) at constant σ_a = 400 MPa. Figure 4.8 (b) shows the effect of σ_m at constant σ_a = 450 MPa. For σ_m = 100 MPa and σ_a = 450 MPa strain accumulation is 0.37%. When σ_m is increased to 150 MPa, strain accumulation is increased to 10.56%. In case of σ_m= 200 MPa, strain accumulation is 16.35%. Increase of ε_r with increasing σ_m level of 100, 150, 200 MPa at constant σ_a = 400 MPa is explained by histogram shown in Figure 4.9.

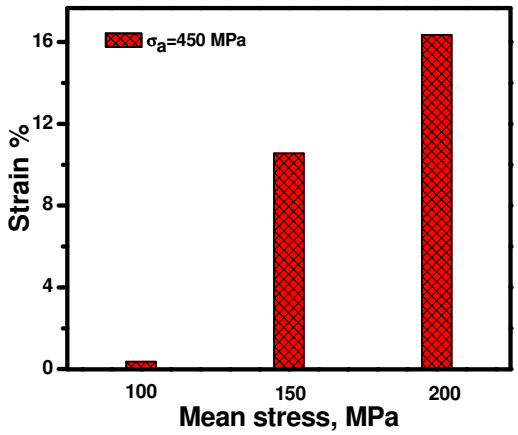

Fig.4.9: Histogram showing the variation of ε_r for σ_m (100,150 and 200 MPa) at constant σ_a (450 MPa).

4.5.3 Strain accumulation: Effect of stress amplitude at constant mean stress

The variation of ratcheting strain (ε_r) with number of cycles for varying σ_a = 400, 450, 500 MPa at constant σ_m = 150, 200 MPa is examined. A typical plot of ε_r vs. N is shown in figure 4.10 (a) at constant σ_m = 150MPa and varying σ_a = 400, 450,500 MPa for 50 cycles. Figure 4.10 (b) shows a typical plot of ε_r vs. N at constant σ_m = 200 MPa and varying σ_a = 400, 450,500 MPa for 50 cycles.

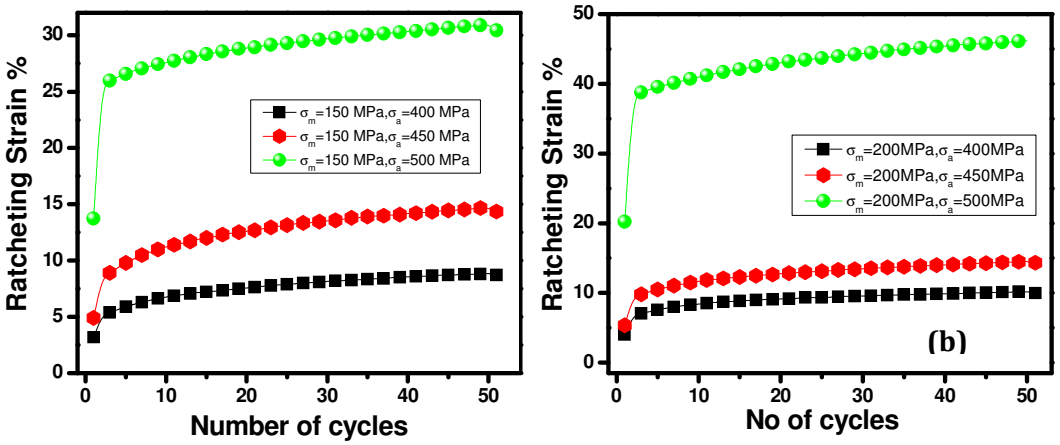

Fig.4.10: Variations of ε_r with number of cycles for (a) σ_a (400,450 and 500 MPa) at constant σ_m (150 Mpa) (b) σ_a (400,450 and 500 MPa) at constant σ_m (200 MPa) after 50 cycles.

The results indicate that ratcheting strain increases monotonically with increase in number of cycles for any σ_a -σ_m combination. The cyclic loading stopped at 50 cycles. Histogram presented in Figure 4.11 clearly shows the increase of ε_r with number of cycles at constant σ_m =150 MPa for 50 cycles. For σ_m =150 MPa and σ_a = 400 MPa strain accumulation is 8.70 %. Strain accumulation increases to 14.34% and 30.42% with increasing of σ_a from 450 MPa to 500 MPa. On increasing the σ_a, maximum stress (σ_{max}) increases while minimum stress (σ_{min}) decreases. Due to this area of hysteresis loop increases. Shifting of hysteresis loop is observed in more strain direction with increasing number of cycles. It is observed from the existing database that strain accumulation increases due to dislocation density (23). Due to shifting of hysteresis loop dislocation density is increasing. Increased area of hysteresis loop causes the increased strain accumulation with σ_a.

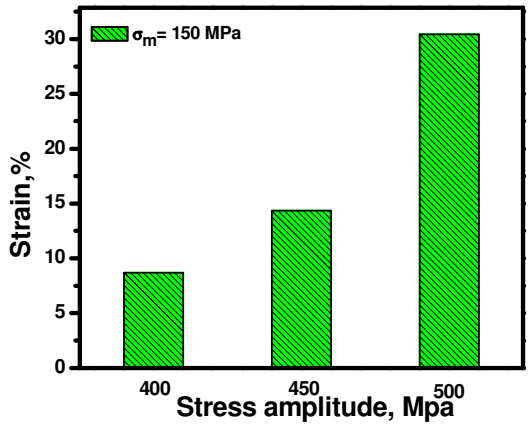

Fig.4.11: Histogram showing the variation of ε_r for σ_a (400,450 and 500 MPa) at constant σ_m (150 MPa).

To study the strain accumulation behavior for 100 cycles similar tests have been done under different combination of σ_m = 150, 200 MPa and σ_a = 400, 450, 500 MPa. Figure 4.12 (a) and Figure 4.12 (b) illustrate the effect of σ_a (400,450,500 MPa) at constant level of σ_m = 150 and 200 MPa on ε_r respectively. Figure 4.12 (a) shows that ratcheting strain accumulation is found to be 5.96 % for σ_m= 150 MPa and σ_a = 400 MPa. With increase in stress amplitude σ_a = 450 MPa strain accumulation increases to 10.26 %. When σ_m = 500 MPa strain accumulation is 10.56 %. Figure 4.12 (b) represents the effect of σ_a (400,450,500 MPa) at

constant σ_m= 200MPa; the values of accumulation of ratcheting strain are 15.82%, 16.34 % and 26.86 % respectively. In this case ε_r increasing with number of cycles for all values of σ_a = 400 MPa, 450 MPa and 500 MPa.

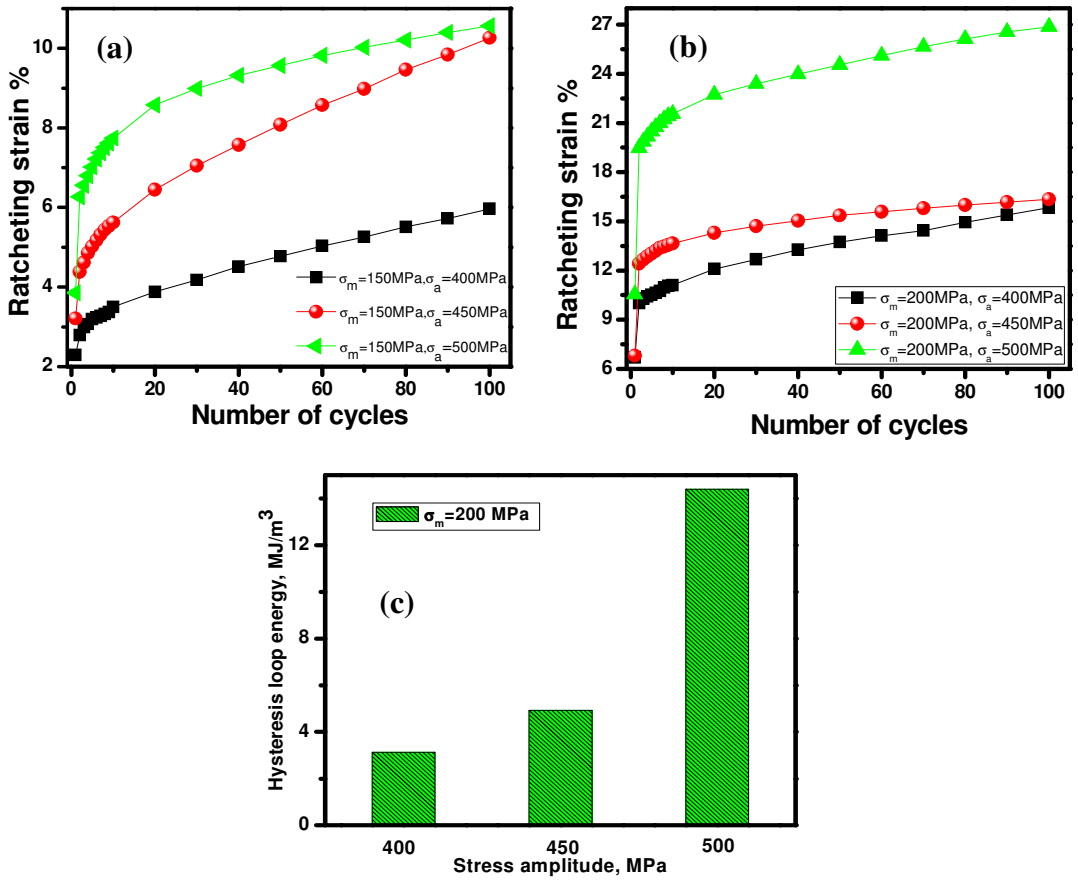

Fig.4.12: Variations of ε_r with number of cycles (a) For σ_a (400, 450 and 500 MPa) at constant σ_m (150 MPa) (b) For σ_a (400, 450, 500 MPa) at constant σ_m (200 MPa) after 100 cycles. (c) Histogram showing variation of loop energy for σ_a (400, 450 and 500MPa) at constant σ_m (200 MPa)

The increase in strain accumulation with σ_a can also be described by using variations in cyclic damage of the investigated material. Damage can be accessed by calculating the energy associated with cyclic deformation, which is calculated by measuring the area under a

particular hysteresis loop for different loading conditions. Figure 4.12 (c) is such a representation for mean stress σ_m= 200 MPa and varying stress amplitude σ_a = 400, 450 and 500 MPa. It is clear from this figure that energy increases with increase in stress amplitude, thus material experiences more cyclic damage and so ratcheting strain increases. Similar increase in loop energy has been noticed for all other employed combination of mean stress and stress amplitude.

4.5.4 Saturation of ratcheting strain

It is known that ratcheting deformation takes place at different rates during the cyclic loading operation [20]It is reported that the rate of accumulation of ratcheting strain is very sharp at initial few cycles of asymmetrical cyclic loading, which eventually becomes saturated attaining a steady sate in strain accumulation; analogous to strain rate -time curves of creep deformation. The phenomenon of attaining a steady state in strain accumulation during ratcheting is commonly known as stable ratcheting or can be termed as plastic shake down when ratcheting strain accumulation tends to be zero [78,79]. Typical variations in rate of accumulation of ratcheting strain ($d\varepsilon_r/dN$) with number of cycles for the investigated non-conventional stainless steel are shown in Figure 4.13 for 100 cycles.

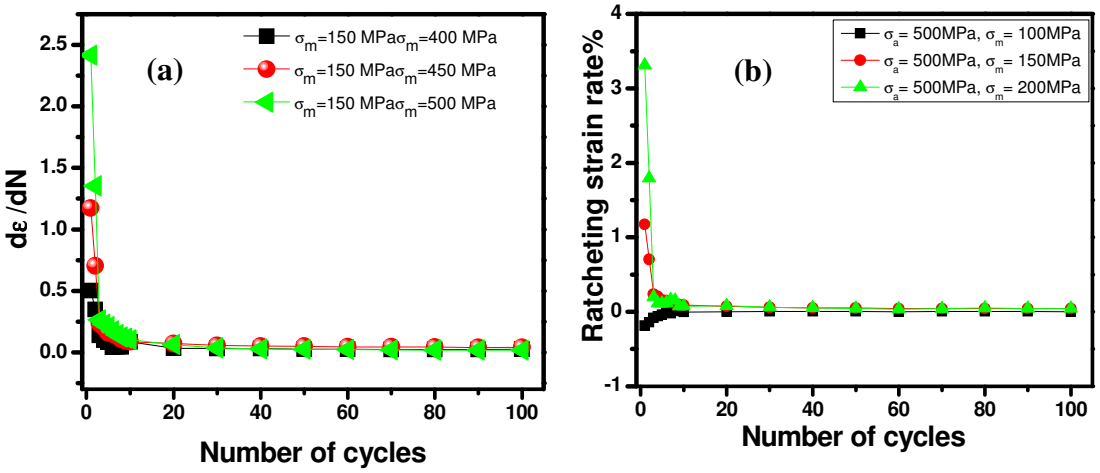

Fig.4.13: Rate of strain accumulation with number of cycles (a) For σ_a (400, 450 and 500 MPa) at constant σ_m (150 MPa) (b) For σ_m (100, 150 and 200 MPa) at constant σ_a (500 MPa) after 100 cycles.

Figure 4.13 (a) shows the plots of rate of accumulation of ratcheting strain with number of cycles for the conditions of σ_m = 150 MPa and σ_a = 400, 450 and 500 MPa. Plots of ($d\varepsilon_r/dN$) with number of cycles for the conditions of σ_a = 500 MPa and σ_m = 100,150 and 200 MPa is shown in figure 4.13 (b).The results in Fig. 4.13 indicate that $d\varepsilon_r/dN$ decreases sharply during the initial few cycles and attains a saturation plateau after 60 cycles for all combinations of σ_m and σ_a . It can be inferred that rapid accumulation of ratcheting strain in the initial few cycles followed by attainment of a steady state value in $d\varepsilon_r/dN$ are the characteristic features of the asymmetric cyclic deformation behavior of investigated non-conventional stainless steel. Figure 4.14 shows the plots of rate of accumulation of ratcheting strain with number of cycles for the conditions of σ_m = 150 MPa and σ_a = 400, 450 and 500 MPa for 50 cycles. Similar phenomena have been observed for all ratcheting experiments irrespective of applied combinations of σ_m and σ_a. The observed nature of attaining steady state in strain accumulation is similar to that observed in existing literature for annealed 42CrMo [80] and interstitial free steel [45]. Based on the attainment of steady state, experiments on the investigated non-conventional stainless steel have been carried out upto 50 and 100 cycles.

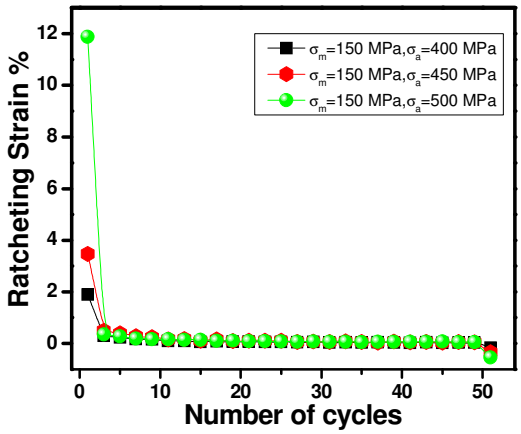

Fig.4.14: Rate of strain accumulation with number of cycles for σ_a (400, 450 and 500 MPa) at constant σ_m (150 MPa) after 50 cycles

The attainment of steady state in $d\varepsilon_r/dN$ can be explained by the nature of dislocation activity which is generated during cyclic deformation. It can be visualized that when a metal is subjected to deformation, whether it is monotonic or cyclic loading, dislocations get

generated which results in strain hardening. The generated dislocations initially form tangles which follow by formation of dislocation cells with increase in number of cycles [24]. After certain number of cycles, depending on the magnitude of accumulated cyclic strain, the newly generated dislocations assume a relatively stable configuration which leads to initiations of the steady state in rate of strain accumulation.

4.5.5 In-situ variations of Microstructure

It is well known that austenitic stainless steel is metastable upon monotonic and cyclic deformation [67]. Therefore it is expected to happen in the investigated steel also. It has been noticed that there is lack of literature in this direction and hence efforts have been made to understand the nature of microstructural variations upon ratcheting deformation. In view of this, X-ray diffraction experiments have been carried out. Dutta et al. have examined martensitic transformation in AISI 304LN stainless steel during ratcheting deformation. They have done their experiments up to failure of the specimens, and measured martensitic transformation after failure. In comparison, current investigation deals with martensitic transformation in intermediate states (after 50 and 100 cycles) of deformation.

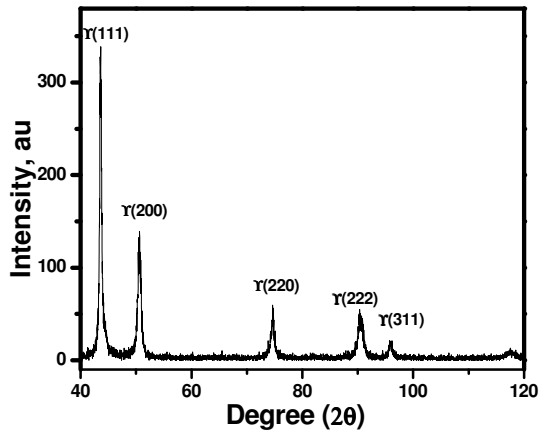

Fig.4.15: X-ray diffraction analysis of unreformed specimen.

A series of X-ray diffraction experiments have been carried out for all the ratcheted specimens of the investigated stainless steel after 50 and 100 cycles of loading on transverse section of the gauge portion. These have been done to understand the extent of deformation

on the microstructure of the investigated stainless steel. Figure 4.15 shows the results of X-ray diffraction analysis of the un-deformed specimen. On the other hand typical results obtained from the X-ray diffraction studies of ratcheted specimens are shown in Figure 4.16 and Figure 4.17 for 50 cycles, Figure 4.18and Figure 4.19 for 100 cycles. The obtained results of X-ray diffraction have been analyzed to quantitatively determine the volume fraction of transformed phase using the equation (2.10) as pointed out in Section 2.10.

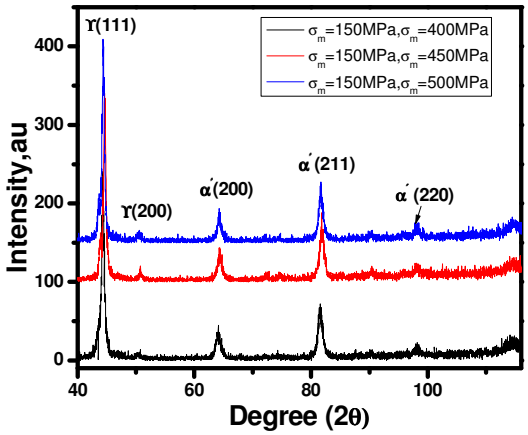

Fig. 4.16: X-ray diffraction analysis for σ_a (400, 450 and 500 MPa) at constant σ_m (150 MPa) after 50 cycles.

Volume fractions of deformed martensite for all the ratcheted samples are listed in Table 4.4. Figure 4.20 and Figure 4.21 show the plots of volume fraction (%) vs. different combinations of σ_m- σ_a for 100 cycles and 50 cycles respectively. The nature of variations in the volume fraction of deformation induced martensite with varying σ_a values at constant σ_m of 100 MPa is shown in Figure 4.20 (a) and that for σ_m =150 MPa is shown in Figure 4.20 (b). In a similar manner, variation in volume fraction of deformation induced martensite with increasing σ_m at constant σ_a values are plotted and illustrated in Figure 4.20 (c) and 4.20 (d). Similar figures are presented in Figure 4.21.

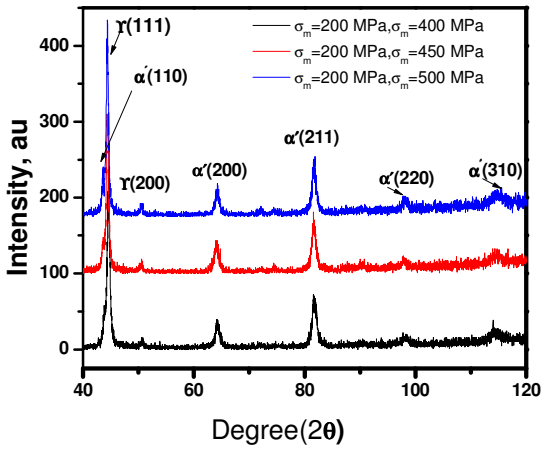

Fig.4.17: X-ray diffraction analysis for σ_a (400, 450 and 500 MPa) at constant σ_m (200 MPa) after 50 cycles

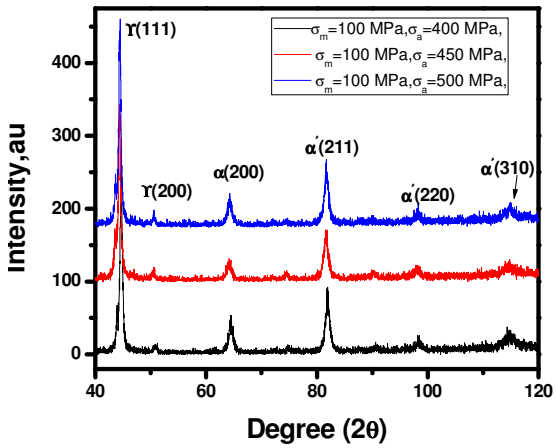

Fig.4.18: X-ray diffraction analysis for σ_a (400, 450 and 500 MPa) at constant σ_m (100 MPa) after 100 cycles.

Several investigators have examined the nature of phase transformation of austenitic steels upon cyclic loading. Only a few researchers have reported on phase transformation of austenitic stainless steel associated with quantitative measurement of volume fraction of the transformed phases under stress controlled cyclic loading. C.Müller et al. have worked on fatigue behavior of austenitic stainless steel [81]. They have concluded that martensite, which formed during cyclic deformation, strongly influences the fatigue limit and causes a strong sensitivity of fatigue limit to the test conditions. M. Grosse et al has done investigation on low cycle fatigue behavior of AISI 321 steel [82]. They have reported that volume fraction of martensite is influenced by strain amplitude, number of cycles and LCF test temperature.

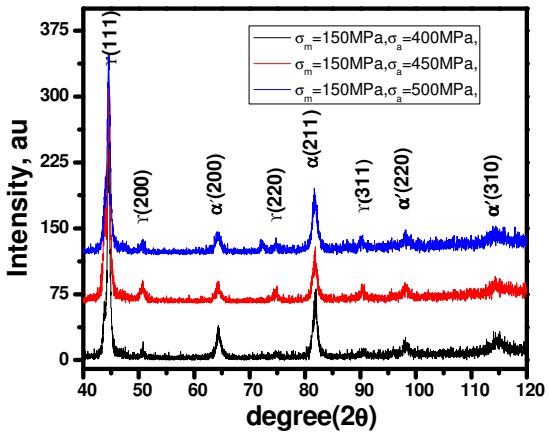

Fig.4.19: X-ray diffraction analysis for σ_a (400, 450 and 500 MPa) at constant σ_m (150 MPa) after 100 cycles.

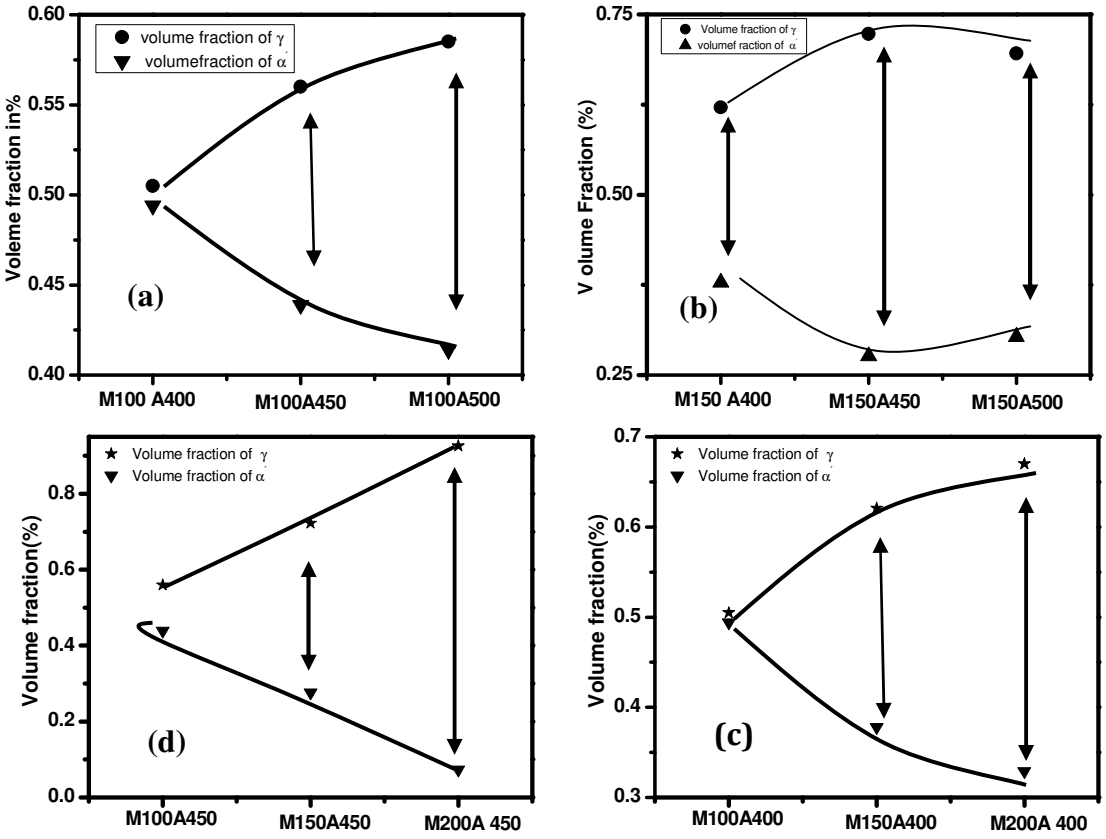

Fig.4.20: Variations of volume fraction with (a) σ_a (400, 450 and 500 MPa) at constant σ_m (100 MPa) (b) σ_a (400, 450 and 500 MPa) at constant σ_m (150 MPa) (c) σ_m (100, 150 and 200 MPa) at constant σ_a (400 MPa) (d) σ_m (100, 150 and 200 MPa) at constant σ_a (450 MPa) after 100 cycles. Arrows indicate increase volume fractions.

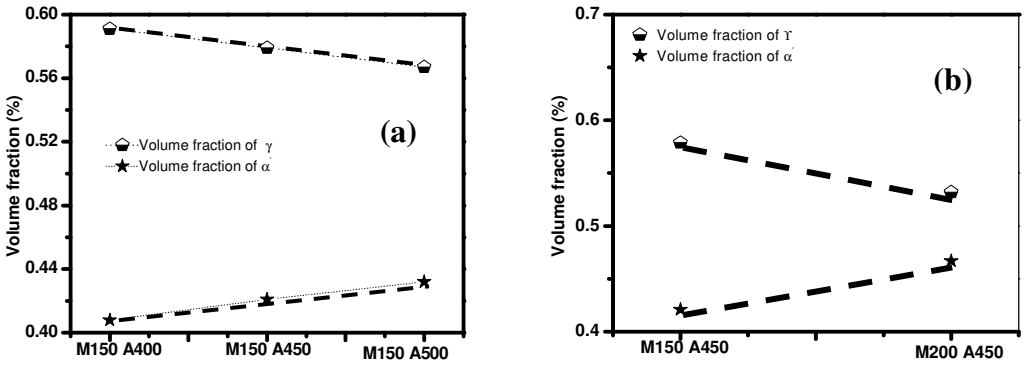

Fig.4.21: Variations of volume fraction with (a) σ_a (400, 450 and 500 MPa) at constant σ_m (150 MPa) (b) σ_m (150 and 200 MPa) at constant σ_a (450 MPa) after 50 cycles. Dotted lines indicate increase in volume fractions.

According to them there is no infuse of LCF frequency on deformed martensite. U. Krupp et al. have worked on chemical composition and fatigue behavior of austenitic stainless steel [83]. They have concluded that fatigue at sub- zero temperature stabilizes the austenite phase for the benefit of α' martensite formation.

Table 4.4 (a) shows volume fractions of deformed martensite after 50 cycles, which shows that volume fraction of deformation induced martensite increases with increase in mean stress/ stress amplitude. Volume fractions of deformed martensite after 100 cycles are listed in Table 4.4 (b). Interestingly for 100 cycles, the variations in volume fractions do not follow any certain trends. This might be due to steady state accumulation of ratcheting strain.

Table 4.4 (a): Volume fractions of deformed martensite after 50 cycles.

Mean stress (σ_m)	**Stress amplitude (σ_a)**	**Volume fraction of (α')martensite**	**Volume fraction of (ϒ) austenite**
150	400	0.408	0.5915
	450	0.421	0.579
	500	0.432	0.567
200	400	0.304	0.695
	450	0.44	0.558
	500	0.467	0.532

Table 4.4 (b): Volume fractions of deformed martensite after 100 cycles.

Mean stress (σ_m)	Stress amplitude (σ_a)	Volume fraction of (α')martensite	Volume fraction of (Υ) austenite
100	400	0.494	0.505
	450	0.439	0.560
	500	0.414	0.585
150	400	0.378	0.621
	450	0.276	0.723
	500	0.303	0.696
200	400	0.329	0.670
	450	0.479	0.521
	500	0.444	0.556

4.6 Post ratcheting hardness test

To assess the extent of deformation during cyclic loading, post-ratcheting hardness tests have been carried out on ratcheted samples. It has been noticed that hardness values of the investigated non-conventional stainless steel specimens increase after ratcheting deformation. Increase in hardness can be considered as due to combined effect of strain hardening due to deformation as well as due to transformation of metastable FCC austenite to stable BCT martensite. Vickers microhardness of the ratcheted specimens is being listed in Table 4.5 and Table 4.6 for 50 and 100 cycles respectively. It is clear from the table that hardness varies with number of cycles. Wide range of hardness variations indicates formation of deformation induced martensite at several places of the section under examination.

Table 4.5: Post ratcheting Microhardness values of the investigated steel after 50 cycles.

Material	D_1 (µm)	D_1 (µm)	$Hv_{0.050}$
ISO/TR 15510 X12CrMnNiN17-7-5 SS	18.75	18.42	268.4
	20.26	21.10	216.8
	19.35	18.20	263
	18.29	19.69	257.1
	18.40	18.40	267

Table 4.6: Post ratcheting Microhardness values of the investigated steel after 100 cycles

Material	D_1 (µm)	D_2 (µm)	$Hv_{0.050}$
ISO/TR 15510 X12CrMnNiN17-7-5 SS	19.45	18.65	255.5
	21.08	20.98	209.8
	18.28	18.73	270.8
	20.27	21.25	215.1
	17.42	17.78	299.3
	18.57	18.47	270.3

Figure 4.22 (a) and Figure 4.22 (b) show the SEM and optical image of ratcheted specimen respectively. Hardness of the transformed martensite is shown by circular area drawn on both figures.

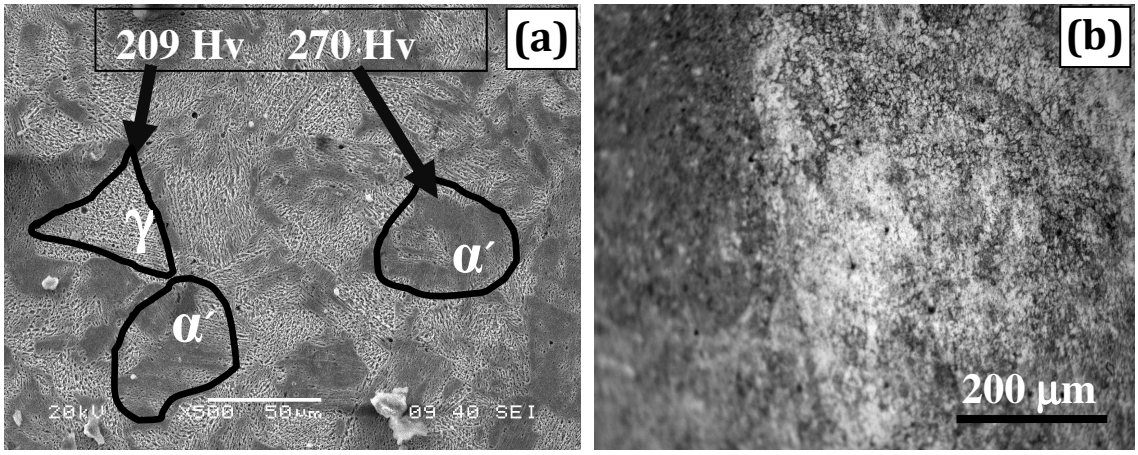

Fig.4.22: (a) SEM image (b) Optical image of ratcheted specimen

In summary, ratcheting deformation of a non- conventional stainless steel (ISO/TR 15510 X12CrMnNiN17-7-5) is carried out in this investigation, where applied asymmetric cyclic loadings lead to phase transformation of austenite to martensite. Strain accumulation due to ratcheting increases with increase in mean stress/ stress amplitude. On the other hand Volume fractions of transformed phases vary with mean stress/ stress amplitude.

CHAPTER 5

CONCLUSIONS AND SCOPE FOR FUTURE RESEARCH

Conclusions and Scope for Future Research

5.1 Conclusions

The obtained results and their pertinent analyses related to ratcheting behavior of ISO/TR 15510 X12CrMnNiN17-7-5 stainless steel and its associated variations in microstructure assist to infer

1. Accumulation of ratcheting strain increases with increasing stress amplitude at constant levels of mean stress values. This fact is considered to occur due to increase in dislocation density with increased cyclic damage of the material. Increment in cyclic damage occurs due to increase in associated hysteresis loop energy and increase in dislocation density can be explained to happen due to shifting of hysteresis loops. In a similar manner, it can be stated that strain accumulation increases when mean stress is increased at constant stress amplitude values.

2. Accumulation of ratcheting strain in the investigated non-conventional stainless steel attains a saturation level after initial 60-70 cycles. Occurrence of this phenomenon is considered to happen due to formation of stable dislocation configuration in the sub structure of the material.

3. Ratcheting deformation results in formation of deformation induced martensite in the investigated non-conventional austenitic stainless steel. This fact is confirmed by X-ray diffraction studies of ratcheted and un-ratcheted specimens. Post-ratcheting hardness measurements lead to infer that Vickers microhardness of the ratcheted samples increases. The reason for the increment in hardness of the material is due to cyclic hardening and formation of martensitic phase in the ratcheted samples; this is attributed to large variations in the microhardness values of the ratcheted samples.

4. Quantitative assessment of volume fraction of the transformed phases states that amount of α´-martensite increases with increase in mean stress/ stress amplitude for cases when ratcheting deformation was given for 50 cycles. On the other hand, variations in volume fraction of α´-martensite do not follow any particular trend when the specimens were ratcheted for 100 cycles. But above all, minimum volume fraction of transformed martensite is about 30%.

5.2Scope for Future Research

1) In the present investigation ratcheting fatigue behavior of a non-conventional austenitic stainless steel have been studied. To study the micro-mechanism associated with ratcheting deformation, TEM analysis should be done; but this has not been done in this study and therefore, it could be of interest for future research.
2) Studies related to post fatigue tensile properties could also improve ratcheting literature.
3) Ratcheting and low cycle fatigue interaction of the investigated material is another direction of work.
4) Some effort towards simulation of ratcheting may also be made by the future researchers.

References

1 Kulkarni, S.C., Desai, Y.M., Kant, T., Reddy, G. R., Parulekar, Y. and Vaze, K.K. (2003), Uniaxial and biaxial ratchetting study of SA333 Gr.6 steel at room temperature, International Journal of Pressure Vessels and Piping, Vol. 80, pp. 179–185.

2 Feaugas, X. and Gaudin, C. (2004), Ratcheting process in the stainless steel AISI 316L at 300 K: an experimental investigation, International Journal of Plasticity, Vol. 20, pp. 643–662.

3 Jiang Y., Sehitoglu H.(1994)., "Cyclic ratcheting of 1070 steel under multiaxial stress states", International Journal of Plasticity, Vol.10, pp. 579-608.

4 Chen X. and Jiao R (2004), Modified kinematic hardening rule for multiaxial ratcheting prediction, International Journal of Plasticity, Vol. 20, pp. 871–898.

5 Bairstow, L. (1911), The elastic limits of iron and steel under cyclical variations of stress, Philosophical Transaction of Royal Society, Vol. 210, pp. 359–386.

6 Kawashima, F., Ishikawa, A. and Asada, Y. (1999), Ratcheting deformation of advanced 316 steel under creep–plasticity condition, Nuclear Engineering and Design, Vol. 193, pp. 327–336.

7 Gao, Q., Kang, G.Z. and Yang, X.J. (2003), Uniaxial ratcheting of SS304 stainless steel at high temperatures: visco-plastic constitutive model, Theoretical and Applied Fracture Mechanics, Vol. 40, pp. 105–111.

8 Yang, Z. and Wang, Z. (1996), Effect of pre strain on cyclic creep behaviour of a high strength spring steel, Materials Science and Engineering A, Vol. 210, pp. 83–93.

9 Gupta C., Chakravartty J. K., Reddy G. R., Banerjee (2005): S., "Uniaxial cyclic deformation behaviour of SA 333 Gr 6 piping steel at room temperature", International Journal of Pressure Vessels and Piping, Vol.82 ,pp. 459–469.

10 Chen, X., Yu, D. and Kim, K. S. (2005), Experimental study on ratcheting behaviour of eutectic tin-lead solder under multiaxial loading, Materials Science Engineering A, Vol. 406, pp. 86–94.

11 Chen, G., Chen, X. and Niu, C.D. (2006), Uniaxial ratcheting behavior of 63Sn37Pb solder with loading histories and stress rates, Materials Science and Engineering A, Vol. 421, pp. 238–244.

12 Lorenzo, F. and Laird, C. (1984), Cyclic creep acceleration and retardation in polycrystalline copper tested at ambient temperature, Acta Metallurgica, Vol. 32. No. 5. pp. 681–692.

13 Lim C.-B., Kim K. S., Seong J. B.(2009), "Ratcheting and fatigue behaviour of a copper alloy under uniaxial cyclic loading with mean stress", International journal of fatigue, Vol.31, pp. 501-507.

14 Kang, G. (2006), Uniaxial Time-dependent Ratcheting of SiCp/6061Al Composites at Room and High Temperature, Composites Science and Technology, Vol. 66, pp. 1418–1430.

15 Chen, X. and Hui, S. (2005), Ratcheting behavior of PTFE under cyclic compression, Polymer Testing, Vol. 24, pp. 829–833.

16 Liu, W., Gao, Z. and Yue, Z. (2008), Steady ratcheting strains accumulation in varying temperature fatigue tests of PMMA, Materials Science and Engineering A, Vol. 492, pp. 102–109.

17 Yoshida, F. (1990), Uniaxial and biaxial creep-ratcheting behaviour of SUS304 stainless steel at room temperature, International Journal of Pressure Vessels & Piping, Vol. 44, pp. 207–223.

18 Kang, G., Gao, Q. and Yang, X. (2002), Uniaxial cyclic ratcheting and plastic flow properties of SS304 stainless steel at room and elevated temperatures, Mechanics of Materials, Vol. 34, pp.145–159.

19 Hassan T., Kyriakides S. (1994), "Ratcheting of cyclically hardening and softening materials: I. Uniaxial behaviour", International Journal of Plasticity, Vol.10, pp. 149-184.

20 Kang G.Z., Li Y.G., Zhang J., Sun Y.F., Gao Q(2005)., "Uniaxial ratcheting and failure behaviours of two steels", Theoretical and Applied Fracture Mechanics,Vol. 43 pp. 199–209.

21 Isobe, N., Sukekawa, M., Nakayama, Y., Date, S., Ohtani, T., Takahashi Y., Kasahara, N., Shibamoto, H., Nagashima, H., Inoue, K .,(2008), Clarification of strain limits considering the ratcheting fatigue strength of 316FR steel, Nuclear Engineering and Design.Vol. 238, pp.347–352.

22 Mizuno M., Mima Y., Karim,A. M. (2000), "Uniaxial ratcheting of 316 FR Steel at room temperature - part 1: Experiments [J], ASME Journal of Engineering Materials and Technology**,** Vol**.**12. pp. 29–34.

23 Tasnim, H., Stelios, K. (1994), "Ratcheting of cyclically hardening and softening materials: I. uniaxial behaviour", International Journal of Plasticity, Vol.10, pp. 149–84.

24 Gaudin, C. and Feaugas, X. (2004), Cyclic creep process in AISI 316L stainless steel in terms of dislocation patterns and internal stresses, Acta Materialia, Vol. 52 pp. 3097–3110.

25 Kang, G., Dong, Y., Liu, Y., Wang, H. and Cheng, X. (2011), Uniaxial ratcheting of 20 carbon steel: Macroscopic and microscopic experimental observations Materials Science and Engineering A, Vol. 528, pp. 5610-5620.

26 Dutta, K., Sivaprasad, S., Tarafder, S. and Ray, K. K. (2010), Influence of asymmetric cyclic loading on substructure formation and ratcheting fatigue behaviour of AISI 304LN stainless steel, Materials Science and Engineering A, Vol. 527, pp. 7571–7579.

27 Ellyin, F. (1997), Fatigue Damage, Crack Growth and Life Prediction, first edition, Chapman & Hall, UK.

28 Dieter, G. E. (1987), Mechanical Metallurgy, SI metric edition, McGraw-Hill Book Company, Singapore

29 Hertzberg, R.W. (1989), Deformation and Fracture Mechanics of Engineering Materials, third edition, John Wiley & Sons, Singapore

30 Suresh, S. (1998), Fatigue of Materials, second edition, Cambridge University Press, UK.

31 Bari, S. and Hassan, T. (2000), Anatomy of coupled constitutive models for ratcheting simulation, International Journal of Plasticity, Vol. 16, pp. 381–409.

32 Karim, M. A. and Ohno, N. (2000), Kinematic hardening model suitable for ratchetting with steady-state, International Journal of Plasticity, Vol. 16, pp. 225–240.

33 Sinha, S. and Ghosh, S. (2006), Modeling cyclic ratcheting based fatigue life of HSLA steels using crystal plasticity FEM simulations and experiments, International Journal of Fatigue, Vol. 28, pp. 1690–1704.

34 Ringsberg, J. W. (2001), Life prediction of rolling contact fatigue crack initiation, International Journal of Fatigue, Vol. 23, pp. 575–586.

35 Satyadevi, A., Sivakumar, S.M. and Bhattacharya, S.S. (2007), A new failure criterion for materials exhibiting ratcheting during very low cycle fatigue, Materials Science and Engineering A, Vol. 452-453, pp. 380–385.

36 Lazan, B. J. (1949) Dynamic creep and rupture properties of temperature-resistant materials under tensile stress, American Society for Testing of Materials, Proceedings, Vol. 49, pp. 757-787.

37 Manjone, M. J. (1949), Effect of pulsating loads on the creep characteristics of aluminum alloy 14S-T, American Society for Testing of Materials, Proceedings, Vol. 49, pp. 788-798.

38 Kenedy, A. J. (1956), Effect of fatigue stresses on creep and recovery, published in the proceedings of International Conference on Fatigue of Metals, Institute of Mechanical Engineers, London, p. 401.

39 Meleka, A. H and Evershed, A. V. (1960), The dependence of creep behavior on the duration of a superimposed fatigue stress, Journal of Institute of Metallurgists, Vol. 88, pp. 411-414.

40 Coffin, L. F., JR. (1960), The stability of metals under cyclic plastic strain, ASME Journal of Basic Engineering, Vol. 82, pp. 671-682.

41 Benham, P. P. (1961), Axial-load and strain-cycling fatigue of copper at low endurance, Journal of Institute of Metals, Vol. 89, p. 328-339.

42 Benham, P. P. and Ford, H. (1961), Low endurance fatigue of a mild steel and an aluminum alloy, Journal of Mechanical Engineering and Sciences, Vol. 3, pp. 119-132.

43 Ruggles, M. B. and Krempl, E. (1990), The interaction of cyclic hardening and ratcheting for AISI type 304 stainless steel at room temperature-I. Experiments, Journal of Mechanics and Physics of Solids, Vol. 38(4) pp. 575–585.

44 Xia, Z., Kujawski, D. and Ellyin, F. (1996), Effect of mean stress and ratcheting strain on fatigue life of steel, International Journal of Fatigue, Vol. 18, pp. 335–341.

45 Van, K.D. and Moumni, Z. (2000), Evaluation of fatigue-ratcheting damage of a pressurized elbow undergoing damage seismic inputs, Nuclear Engineering Designs, Vol. 196, pp. 41–50.

46 Tao, G. and Xia, Z. (2007), Ratcheting behavior of an epoxy polymer and its effect on fatigue life, Polymer Testing, Vol. 26, pp. 451–460.

47 Kang, G., Kan, Q., Qian, L. and Liu, Y. (2009), Ratchetting Deformation of Super-elastic and Shape-memory NiTi alloys, Mechanics of Materials, Vol. 41 pp. 139–153.

48 Dutta,K and Ray, K.K. , (2013), Ratcheting strain in interstitial free steel Materials Science and Engineering A, Vol.575, pp.127–135.

49 Paul, S. K., Sivaprasad, S., Dhar, S. and Tarafder, S. (2010). True stress control asymmetric cyclic plastic behavior in SA333 C–Mn steel, Internatiional Journal of Pressure Vessels and Piping, Vol. 87, pp. 440–446.

50 Chen G., Chen X., Niu C-D ((2010), "Uniaxial ratcheting behaviour of 63Sn37Pb solder with loading histories and stress rates", Materials Science and Engineering A, Vol.421 pp. 238-244.

51 Mcdowell. D.L. ((1998),"Stress rate dependence of cyclic ratcheting behaviour of two rail steels", International Journal of Plasticity, Vol.14, pp. 355-390.

52 Xia Z., Kujawski D., Ellyin F. (1995), "Effect of mean stress and ratcheting strain on fatigue life of steel", International Journal of Fatigue, vol.96, pp. 335-341.

53 Mercer M.E., Dickerson S.L., Gibeling J.C. (1995), "Cyclic deformation of dispersion strengthened aluminium alloys", Materials Science and Engineering A, Vol.203, pp. 46-58.

54 Zhang X.P., Castagne S., Gu C.F., Luo X.F. (2011), "Effects of annealing treatment on the ratcheting behaviour of extruded AZ31B magnesium alloy under asymmetrical uniaxial cyclic loading", Journal of Materials Science, Vol. 46, pp. 1124-1131.

55 Chen G., Shan S-C., Chen X., Yuan H. (2010), "Ratcheting and fatigue properties of the high-nitrogen steel X13CrMnMoN18-14-3 under cyclic loading", Computational Materials Science, vol. 46, pp. 572–578.

56 Kang G., Liu Y., Dong Y. and Gao Q (2011), Uniaxial ratcheting behaviors of metals with different crystal structures or values of fault energy: macroscopic experiments, Journal of Materials Science and Technology, Vol. 27(5), pp. 453-459.

57 Pickard A.C., Knott J.F. (1988), "Effect of testing method on cyclic hardening behaviour in face-centered-cubic alloys, in low cycle fatigue, American Society for Testing and Materials, Philadelphia, PA, pp. 58-76.

58 Wang Q.G., Apelian D., Lados D.A. (2001), "Fatigue behaviour of A356-T6 aluminum cast alloys. Part I. effect of casting defects", Journal of Light Metals, Vol. 1, pp. 73–84.

59 Olson, G.B., Cohen, M., Less,J., (1927), A mechanism for strain induced nucleation of martensitic transformation, Common Metals, Vol.28,pp.107

60 Coubrough, G.J., Matlock, D.K.., Van, C.J., Tyne. (1993), Formability of type 304 stainless sheet, Society of automotive engineers, Vol .930814, pp.279-289.

61 Talonen, J., Nenonen, P., Pap, G and Hanninen, H. (2005), Effect of strain rate on the strain induced c?a0 martensite transformation and mechanical properties of austenitic stainless steels, Metallurgical Transaction, A Vol. 36, pp.421. K

62 Spencer, K., Embury, J.D., ConloN, .K.D., Veron. M., Y, Brechet. (2004), Stregthening via the formation of strain-induced $\gamma \rightarrow \alpha'$ martensite in stainless steels Mater. Sci.Eng. A Vol.387–389, pp. 873.

63 Choi, J.Y and Jin,W. (1997), Strain induced martensite formation and its effect on strain hardening behavior in the cold drawn 304 austenitic stainless steels Scripta Materialia, Vol. 36, pp. 99-104.

64 Lee, W-S., Chi, F Lin.(2000), The morphologies and characteristics of impact-induced martensite in 304L stainless steel Scripta Materialia, Vol. 43, pp. 777-782.

65 Hecker, S.S., Stout, M.G., Staudhammer. K.P and Smith,J.L.(1982),:'Effects of strain state and strain rate on deformation-induced transformation in 304 stainless steel. Part I – magnetic measurements and mechanical behaviour', Metall. Mater. Trans. A, Vol.13A, pp. 619–626.

66 Kumar,A., Singhal,L.K. (1989) ,Effect of strain rate on martensitic transformation during uniaxial testing of AISI 304 stainless steel Metall. Trans, Vol. 20A,pp. 2857.

67 De, A. K., Murdock, D. C., Mataya, M.C., Speer, J. G. and Matlock, D. K. (2000), Quantitative measurement of deformation-induced martensite in 304 stainless steel by X-ray diffraction, Scripta Materialia, Vol. 50, pp. 1445–1449.

68 Nayar, A., The steel hand book, second edition, Tata MC Graw- Hill company limited.

69 E 112-04, (2004), Standard Test Methods for Determining Average Grain Size, Annual Book of ASTM Standards, Vol. 03.01, ASTM, Philadelphia, PA.

70 E8M-08, (2008), Standard Test Methods for Tension Testing of Metallic Materials, Annual Book of ASTM Standards, Vol. 03.01, ASTM, Philadelphia, PA.

71 ASM International Handbook Committee (1999), Stainless Steels, ASM Specialty Handbook, ASM International, Ohio.

72 Thomason, P. F, (1993), ductile fracture by the growth and coalescence of microvoids of non-uniform size and spacing, Acta metall, mater. Vol. 41, No. 7, pp. 2127-2134.

73 Tvergaard, V. (1982), Ductile fracture by cavity nucleation between larger voids, Journal of Mechanics and Physics of Solids, Vol. 30, No. 4, pp. 265–286.

74 Bandstra, J.P., Koss. D.A , (2001) , Modeling the ductile fracture process of void coalescence by void-sheet formation, Materials Science and Engineering A,Vol.319–321,pp. 490–495.

75 Benzerga, A .A ., Besson, J., Pineau, .(2004), Anisotropic ductile fracture Part II:

theory, Acta Materialia,Vol. 52, pp. 4639–4650.

76 Bandstraa, J.P., Kossb, D.A., Maticc, A. P., Everettd, R.K. (2004), Modeling void coalescence during ductile fracture of a steel, Materials Science and Engineering A,Vol.366, pp. 269–281.

77 Ray, K.K., Dutta, K.., Sivaprasad, S. and Tarafder, S. (2010), Fatigue damage of AISI 304 LN stainless steel: Role of mean stress, Procedia Engineering, Vol. 2, pp. 1805–1813.

78 Yang, X. (2005), Low cycle fatigue and cyclic stress ratcheting failure behaviour of carbon steel 45 under uniaxial cyclic loading, International Journal of Fatigue, Vol. 27, pp. 1124–1132.

79 Kang, G., Kan, Q., Qian, L. and Liu, Y. (2009), Ratcheting Deformation of Super-elastic and Shape-memory Ni-Ti alloys, Mechanics of Materials, Vol. 41 pp. 139–153.

80 Kang, G., Liu. Y, Ding, J., Gao, Q,(2009), Uniaxial ratcheting and fatigue failure of tempered 42CrMo steel: Damage evolution and damage-coupled visco-plastic constitutive model, International Journal of Plasticity, Vol. 25, pp.838–860.

81 C, Müller-Bollenhagen., M, Zimmermann., H.-J. Christ. (2010), Very high cycle fatigue behaviour of austenitic stainless steel and the effect of strain-induced martensite, International Journal of Fatigue, Vol. 32, pp. 936–942.

82 M, Grosse ., D, Kalkhof., M, Niffenegger., L. Keller. (2006), Influencing parameters on martensite transformation during low cycle fatigue for steel AISI 321, Materials Science and Engineering A, Vol. 437, pp. 109–113

83 U, Krupp., C, West., H.-J, Christ. (2008), Deformation-induced martensite formation during cyclic deformation of metastable austenitic steel: Influence of temperature and carbon content, Materials Science and Engineering A ,vol.481–482 ,pp.713–717